Nonlinear Dyn (2013) 72:417–438
DOI 10.1007/s11071-012-0725-3

ORIGINAL PAPER

Analytical solutions for asymmetric periodic motions to chaos in a hardening Duffing oscillator

Albert C.J. Luo · Jianzhe Huang

Received: 14 November 2012 / Accepted: 16 December 2012 / Published online: 12 January 2013

Abstract In this paper, the analytical dynamics of asymmetric periodic motions in the periodically forced, hardening Duffing oscillator is investigated via the generalized harmonic balance method. For the hardening Duffing oscillator, the symmetric periodic motions were extensively investigated with the aim of a good understanding of solutions with jumping phenomena. However, the asymmetric periodic motions for the hardening Duffing oscillators have not been obtained yet, and such asymmetric periodic motions are very important to find routes of periodic motions to chaos in the hardening Duffing oscillator analytically. Thus, the bifurcation trees from asymmetric period-1 motions to chaos are presented. The corresponding unstable periodic motions in the hardening Duffing oscillator are presented, and numerical illustrations of stable and unstable periodic motions are carried out as well. This investigation provides a comprehensive understanding of chaos mechanism in the hardening Duffing oscillator.

Keywords Hardening Duffing oscillator · Asymmetric periodic motions · Symmetric periodic motions · Hopf bifurcation · Saddle-node bifurcation

A.C.J. Luo (✉) · J. Huang
Department of Mechanical and Industrial Engineering, Southern Illinois University Edwardsville, Edwardsville, IL 62026-1805, USA
e-mail: aluo@siue.edu

1 Introduction

In mechanical engineering, in 1918, Duffing [1] presented the hardening spring model to describe the vibration of electro-magnetized vibrating beam. Since then, the Duffing oscillator has been extensively used to describe nonlinear structural vibrations in structural dynamics. In 1964, Hayashi [2] discussed the approximate periodic solutions and the corresponding stability by the averaging method and harmonic balance method. In 1973, Nayfeh [3] used the perturbation method to approximate periodic motion of the Duffing oscillators. In 1976, Holmes and Rand [4] discussed the stability and bifurcation of the Duffing oscillator via the catastrophe theory. In 1979, Nayfeh and Mook [5] presented the nonlinearity of the Duffing oscillators in structural vibration through the perturbation analysis, and Holmes [6] showed the strange attractors of chaotic motions in nonlinear oscillators via the Duffing oscillator with a twin-well potential. In 1980, Ueda [7] used numerical simulations to show chaos via period-doubling of periodic motions of Duffing oscillators. In 1990, Coppola and Rand [8] used the method of averaging with elliptic functions to approximately determine the limit cycles of nonlinear oscillators. In 1992, Wang et al. [9] used the harmonic balance method and the Floquet theory to investigate the bifurcation behaviors of the Duffing oscillator with a bounded potential well (also see, Kuo et al. [10]). In 1995, Hanicki and Szemplinski-Stupnicka [11] used the perturbation method to investigate the approximate solutions of periodic motions

in the twin-well potential Duffing oscillator. In 1997, Luo and Han [12] analytically presented the stability and bifurcation conditions of periodic motions of the Duffing oscillator, different from the traditional perturbation analysis. However, the constant term of the analytical solution for the steady-state motion of the Duffing oscillator was not considered. In 1996, Luo and Han [13] presented an improved solution of the Duffing oscillator with a twin-well potential. For analytical prediction of chaos, in 1999, Luo and Han [14] investigated chaotic motions in nonlinear rods through the Duffing oscillator. In 2008, Peng et al. [15] presented the approximate period-1 solution for the Duffing oscillator by the harmonic balance method with three harmonic terms, compared with the fourth-order Runge-Kutta method. In 2012, Luo and Huang [16] presented a generalized harmonic balance method to obtain the analytical solution of period-1 motion of the Duffing oscillator with a twin-well potential. Luo and Huang [17] also presented a generalized harmonic balance method to determine period-m solutions in such a Duffing oscillator. The hardening Duffing oscillator possesses dynamical behaviors different from the Duffing oscillator with the twin-well. So far, one only knows symmetric periodic motions with a rough approximation for the hardening Duffing oscillator. The asymmetric periodic motions in such hardening oscillator are not discussed yet. Herein, such asymmetric periodic motions will be discussed analytically because the asymmetric periodic motions are a key to find the route to chaos analytically.

In this paper, the generalized harmonic balance method will be used to investigate analytical periodic motions in the periodically forced, hardening Duffing oscillator. The symmetric and asymmetric period-1 motions for such a Duffing oscillator will be investigated and the corresponding analytical solutions will be presented. The stability and bifurcations of such period-1 motions will be carried out. The bifurcation tree from asymmetric period-1 motions to period-4 motions will be presented. The corresponding unstable periodic motions in the hardening Duffing oscillator will be presented. Numerical illustrations of stable and unstable periodic motions will be carried out.

2 Formulation

Consider a hardening Duffing oscillator

$$\ddot{x} + \delta\dot{x} + \alpha x + \beta x^3 = Q_0 \cos \Omega t \tag{1}$$

where $\dot{x} = dx/dt$ is velocity. Q_0 and Ω are excitation amplitude and frequency, respectively. δ is damping coefficient. α and β are linear and nonlinear stiffness coefficients of the Duffing oscillator. From Eq. (1), the standard form for the Fourier analysis is

$$\ddot{x} = f(x, \dot{x}, t) \tag{2}$$

where

$$f(x, \dot{x}, t) = -\delta\dot{x} - \alpha x - \beta x^3 + Q_0 \cos \Omega t. \tag{3}$$

In 2012, Luo [18] presented a generalized harmonic balance method to obtain analytical periodic motions. From such a generalized harmonic balance method, the analytical solution of period-1 motion for the hardening Duffing oscillator is

$$x^*(t) = a_0(t) + \sum_{k=1}^{N} b_k(t)\cos(k\Omega t) + c_k(t)\sin(k\Omega t) \tag{4}$$

and the analytical solution of period-m motion for such a Duffing oscillator is

$$x^*(t) = a_0^{(m)}(t) + \sum_{k=1}^{N} b_{k/m}(t)\cos\left(\frac{k}{m}\Omega t\right) + c_{k/m}(t)\sin\left(\frac{k}{m}\Omega t\right). \tag{5}$$

For $m = 1$, the period-1 motion given in Eq. (3) is recovered. From Eq. (5), the first and second order derivatives of $x^*(t)$ are

$$\dot{x}^*(t) = \dot{a}_0^{(m)} + \sum_{k=1}^{N}\left(\dot{b}_{k/m} + \frac{k\Omega}{m}c_{k/m}\right)\cos\left(\frac{k}{m}\Omega t\right) + \left(\dot{c}_{k/m} - \frac{k\Omega}{m}b_{k/m}\right)\sin\left(\frac{k}{m}\Omega t\right), \tag{6}$$

$$\ddot{x}^*(t) = \ddot{a}_0^{(m)} + \sum_{k=1}^{N}\left(\ddot{b}_{k/m} + 2\frac{k\Omega}{m}\dot{c}_{k/m} - \left(\frac{k\Omega}{m}\right)^2 b_{k/m}\right)\cos\left(\frac{k}{m}\Omega t\right) + \left(\ddot{c}_{k/m} - 2\frac{k\Omega}{m}\dot{b}_{k/m} - \left(\frac{k\Omega}{m}\right)^2 c_{k/m}\right) \times \sin\left(\frac{k}{m}\Omega t\right). \tag{7}$$

Substitution of Eqs. (4)–(7) to Eq. (2) and using the coefficients of the Fourier series for all terms of $\cos(k\Omega t/m)$ and $\sin(k\Omega t/m)$ gives

$$\begin{aligned}
&\ddot{a}_0^{(m)} = F_0^{(m)}\big(a_0^{(m)}, \mathbf{b}^{(m)}, \mathbf{c}^{(m)}, \dot{a}_0^{(m)}, \dot{\mathbf{b}}^{(m)}, \dot{\mathbf{c}}^{(m)}\big),\\
&\ddot{b}_{k/m} + 2\frac{k\Omega}{m}\dot{c}_{k/m} - \left(\frac{k\Omega}{m}\right)^2 b_{k/m}\\
&\quad = F_{1k}^{(m)}\big(a_0^{(m)}, \mathbf{b}^{(m)}, \mathbf{c}^{(m)}, \dot{a}_0^{(m)}, \dot{\mathbf{b}}^{(m)}, \dot{\mathbf{c}}^{(m)}\big),\\
&\ddot{c}_{k/m} - 2\frac{k\Omega}{m}\dot{b}_{k/m} - \left(\frac{k\Omega}{m}\right)^2 c_{k/m}\\
&\quad = F_{2k}^{(m)}\big(a_0^{(m)}, \mathbf{b}^{(m)}, \mathbf{c}^{(m)}, \dot{a}_0^{(m)}, \dot{\mathbf{b}}^{(m)}, \dot{\mathbf{c}}^{(m)}\big),\\
&\quad k = 1, 2, \ldots, N.
\end{aligned} \tag{8}$$

The coefficients of $\cos k\Omega t$ and $\sin k\Omega t$ for the function of $f(x, \dot{x}, t)$ are

$$\begin{aligned}
&F_0^{(m)}\big(a_0^{(m)}, \mathbf{b}^{(m)}, \mathbf{c}^{(m)}, \dot{a}_0^{(m)}, \dot{\mathbf{b}}^{(m)}, \dot{\mathbf{c}}^{(m)}\big)\\
&\quad = -\delta\dot{a}_0^{(m)} - \alpha a_0^{(m)} - \beta f_0^{(m)};\\
&F_{1k}^{(m)}\big(a_0^{(m)}, \mathbf{b}^{(m)}, \mathbf{c}^{(m)}, \dot{a}_0^{(m)}, \dot{\mathbf{b}}^{(m)}, \dot{\mathbf{c}}^{(m)}\big)\\
&\quad = -\delta\left(\dot{b}_{k/m} + \frac{k\Omega}{m}c_{k/m}\right) - \alpha b_{k/m}\\
&\qquad - \beta f_k^{(c)} + Q_0\delta_k^m;\\
&F_{2k}^{(m)}\big(a_0^{(m)}, \mathbf{b}^{(m)}, \mathbf{c}^{(m)}, \dot{a}_0^{(m)}, \dot{\mathbf{b}}^{(m)}, \dot{\mathbf{c}}^{(m)}\big)\\
&\quad = -\delta\left(\dot{c}_{k/m} - \frac{k\Omega}{m}b_{k/m}\right) - \alpha c_{k/m} - \beta f_k^{(s)}
\end{aligned} \tag{9}$$

where the nonlinear coefficient functions are

$$\begin{aligned}
f_0^{(m)} = {} & \big(a_0^{(m)}\big)^3 + \sum_{l=1}^{N}\sum_{j=1}^{N}\sum_{i=1}^{N}\Bigg[\frac{3a_0^{(m)}}{2N}b_{i/m}b_{j/m}\delta_{i-j}^0\\
& + \frac{3a_0^{(m)}}{2N}c_{i/m}c_{j/m}\delta_{i-j}^0\\
& + \frac{1}{4}b_{i/m}b_{j/m}b_{l/m}\big(\delta_{i-j-l}^0 + \delta_{i-j+l}^0 + \delta_{i+j-l}^0\big)\\
& + \frac{3}{4}b_{i/m}c_{j/m}c_{l/m}\big(\delta_{i+j-l}^0 + \delta_{i-j+l}^0\\
& - \delta_{i-j-l}^0\big)\Bigg],
\end{aligned} \tag{10}$$

$$\begin{aligned}
f_k^{(c)} = {} & \sum_{l=1}^{N}\sum_{j=1}^{N}\sum_{i=1}^{N}\Bigg[3\left(\frac{a_0^{(m)}}{N}\right)^2 b_{l/m}\delta_l^k\\
& + \frac{3a_0^{(m)}}{2N}b_{l/m}b_{j/m}\big(\delta_{|l-j|}^k + \delta_{l+j}^k\big)\\
& + \frac{3a_0^{(m)}}{2N}c_{l/m}c_{j/m}\big(\delta_{|l-j|}^k - \delta_{l+j}^k\big)\\
& + \frac{1}{4}b_{l/m}b_{j/m}b_{i/m}\big(\delta_{|l-j-i|}^k + \delta_{l+j+i}^k\\
& + \delta_{|l-j+i|}^k + \delta_{|l+j-i|}^k\big)\\
& + \frac{3}{4}b_{l/m}c_{j/m}c_{i/m}\big(\delta_{|l+j-i|}^k - \delta_{l+j+i}^k\\
& + \delta_{|l-j+i|}^k - \delta_{|l-j-i|}^k\big)\Bigg],
\end{aligned} \tag{11}$$

$$\begin{aligned}
f_k^{(s)} = {} & \sum_{l=1}^{N}\sum_{j=1}^{N}\sum_{i=1}^{N}\Bigg[3\left(\frac{a_0^{(m)}}{N}\right)^2 c_{l/m}\delta_l^k\\
& + \frac{3a_0^{(m)}}{N}b_{l/m}c_{j/m}\big[\delta_{l+j}^k - \operatorname{sgn}(l-j)\delta_{|l-j|}^k\big]\\
& + \frac{1}{4}c_{l/m}c_{j/m}c_{i/m}\big[\operatorname{sgn}(l-j+i)\delta_{|l-j+i|}^k\\
& - \delta_{l+j+i}^k + \operatorname{sgn}(l+j-i)\delta_{|l+j-i|}^k\\
& - \operatorname{sgn}(l-j-i)\delta_{|l-j-i|}^k\big]\\
& + \frac{3}{4}b_{l/m}b_{j/m}c_{i/m}\big[\operatorname{sgn}(l-j+i)\delta_{|l-j+i|}^k\\
& + \delta_{l+j+i}^k - \operatorname{sgn}(l+j-i)\delta_{|l+j-i|}^k\\
& - \operatorname{sgn}(l-j-i)\delta_{|l-j-i|}^k\big]\Bigg].
\end{aligned} \tag{12}$$

Let

$$\begin{aligned}
\mathbf{z}^{(m)} &\triangleq \big(a_0^{(m)}, \mathbf{b}^{(m)}, \mathbf{c}^{(m)}\big)^{\mathrm{T}}\\
&= \big(a_0^{(m)}, b_{1/m}, \ldots, b_{N/m}, c_{1/m}, \ldots, c_{N/m}\big)^{\mathrm{T}}\\
&\equiv \big(z_0^{(m)}, z_1^{(m)}, \ldots, z_{2N}^{(m)}\big)^{\mathrm{T}},\\
\mathbf{z}_1 = \dot{\mathbf{z}} &= \big(\dot{a}_0^{(m)}, \dot{\mathbf{b}}^{(m)}, \dot{\mathbf{c}}^{(m)}\big)^{\mathrm{T}}\\
&= \big(\dot{a}_0^{(m)}, \dot{b}_{1/m}, \ldots, \dot{b}_{N/m}, \dot{c}_{1/m}, \ldots, \dot{c}_{N/m}\big)^{\mathrm{T}}\\
&\equiv \big(\dot{z}_0^{(m)}, \dot{z}_1^{(m)}, \ldots, \dot{z}_{2N}^{(m)}\big)^{\mathrm{T}}
\end{aligned} \tag{13}$$

where

$$\mathbf{b}^{(m)} = (b_{1/m}, b_{2/m}, \ldots, b_{N/m})^{\mathrm{T}} \quad \text{and}$$
$$\mathbf{c}^{(m)} = (c_{1/m}, c_{2/m}, \ldots, c_{N/m})^{\mathrm{T}}. \tag{14}$$

Equation (8) can be expressed in the vector form of

$$\dot{\mathbf{z}}^{(m)} = \mathbf{z}_1^{(m)} \quad \text{and} \quad \dot{\mathbf{z}}_1^{(m)} = \mathbf{g}^{(m)}\left(\mathbf{z}^{(m)}, \mathbf{z}_1^{(m)}\right) \tag{15}$$

where

$$\begin{aligned}
&\mathbf{g}^{(m)}\left(\mathbf{z}^{(m)}, \mathbf{z}_1^{(m)}\right) \\
&= \left(-F_0^{(m)}\left(\mathbf{z}^{(m)}, \mathbf{z}_1^{(m)}\right) - \mathbf{F}_1^{(m)}\left(\mathbf{z}^{(m)}, \mathbf{z}_1^{(m)}\right)\right. \\
&\quad - 2\frac{\mathbf{k}_1\Omega}{m}\dot{\mathbf{c}}^{(m)} + \mathbf{k}_2\left(\frac{\Omega}{m}\right)^2\mathbf{b}^{(m)} - \mathbf{F}_2^{(m)}\left(\mathbf{z}^{(m)}, \mathbf{z}_1^{(m)}\right) \\
&\quad \left. + 2\frac{\mathbf{k}_1\Omega}{m}\dot{\mathbf{b}}^{(m)} + \mathbf{k}_2\left(\frac{\Omega}{m}\right)^2\mathbf{c}^{(m)}\right)
\end{aligned} \tag{16}$$

and

$$\begin{aligned}
&\mathbf{k}_1 = \mathrm{diag}(1, 2, \ldots, N) \quad \text{and} \\
&\mathbf{k}_2 = \mathrm{diag}\left(1, 2^2, \ldots, N^2\right), \\
&\mathbf{F}_1^{(m)} = \left(F_{11}^{(m)}, F_{12}^{(m)}, \ldots, F_{1N}^{(m)}\right)^{\mathrm{T}} \quad \text{and} \\
&\mathbf{F}_2^{(m)} = \left(F_{21}^{(m)}, F_{22}^{(m)}, \ldots, F_{2N}^{(m)}\right)^{\mathrm{T}} \\
&\quad \text{for } N = 1, 2, \ldots, \infty
\end{aligned} \tag{17}$$

and

$$\mathbf{y}^{(m)} \equiv \left(\mathbf{z}^{(m)}, \mathbf{z}_1^{(m)}\right) \quad \text{and} \quad \mathbf{f}^{(m)} = \left(\mathbf{z}_1^{(m)}, \mathbf{g}^{(m)}\right)^{\mathrm{T}}. \tag{18}$$

Thus, Eq. (15) becomes

$$\dot{\mathbf{y}}^{(m)} = \mathbf{f}^{(m)}\left(\mathbf{y}^{(m)}\right). \tag{19}$$

The solutions of steady-state periodic motion can be obtained by setting $\dot{\mathbf{y}}^{(m)} = \mathbf{0}$, i.e.,

$$\begin{aligned}
&F_0^{(m)}\left(a_0^{(m)*}, \mathbf{b}^{(m)*}, \mathbf{c}^{(m)*}, 0, \mathbf{0}, \mathbf{0}\right) = 0, \\
&\mathbf{F}_1^{(m)}\left(a_0^{(m)*}, \mathbf{b}^{(m)*}, \mathbf{c}^{(m)*}, 0, \mathbf{0}, \mathbf{0}\right) \\
&\quad - \frac{\Omega^2}{m^2}\mathbf{k}_2\mathbf{b}^{(m)*} = \mathbf{0}, \\
&\mathbf{F}_2^{(m)}\left(a_0^{(m)*}, \mathbf{b}^{(m)*}, \mathbf{c}^{(m)*}, 0, \mathbf{0}, \mathbf{0}\right) - \frac{\Omega^2}{m^2}\mathbf{k}_2\mathbf{c}^{(m)*} = \mathbf{0}.
\end{aligned} \tag{20}$$

The $(2N + 1)$ nonlinear equations in Eq. (20) are solved by Newton–Raphson method. The linearized equation at the equilibrium point $\mathbf{y}^{(m)*} = (\mathbf{z}^{(m)*}, \mathbf{0})^{\mathrm{T}}$ is given by

$$\begin{aligned}
&\Delta\dot{\mathbf{y}}^{(m)} = D\mathbf{f}^{(m)}\left(\mathbf{y}^{*(m)}\right)\Delta\mathbf{y}^{(m)} \quad \text{and} \\
&D\mathbf{f}^{(m)}\left(\mathbf{y}^{*(m)}\right) = \partial\mathbf{f}^{(m)}\left(\mathbf{y}^{(m)}\right)/\partial\mathbf{y}^{(m)}\big|_{\mathbf{y}^{(m)*}}.
\end{aligned} \tag{21}$$

The corresponding eigenvalues are determined by

$$\left|D\mathbf{f}^{(m)}\left(\mathbf{y}^{*(m)}\right) - \lambda\mathbf{I}_{2(2N+1)\times 2(2N+1)}\right| = 0. \tag{22}$$

If $\mathrm{Re}(\lambda_k) < 0$ $(k = 1, 2, \ldots, 2(2N + 1))$, the approximate, steady-state, periodic solution $\mathbf{y}^{(m)*}$ with truncation of $\cos(N\Omega t/m)$ and $\sin(N\Omega t/m)$ is stable. If $\mathrm{Re}(\lambda_k) > 0$ $(k \in \{1, 2, \ldots, 2(2N + 1)\})$, the truncated approximate steady-state solution is unstable. The boundary between the stable and unstable solutions is given by the bifurcation condition, including saddle-node bifurcation and Hopf bifurcation.

3 Analytical prediction of periodic solutions

For the symmetric motion, $a_0^{(m)} = 0$ is obtained. For one harmonic term balance, setting $m = k = 1$, Eq. (9) becomes

$$\begin{aligned}
&F_0^{(1)}(a_0, b_1, c_1, \dot{a}_0, \dot{b}_1, \dot{c}_1) = 0, \\
&F_{11}^{(1)}(a_0, b_1, c_1, \dot{a}_0, \dot{b}_1, \dot{c}_1) \\
&\quad = -\delta(\dot{b}_1 + \Omega c_1) - \alpha b_1 - \beta f_1^{(c)} + Q_0, \\
&F_{21}^{(1)}(a_0, b_1, c_1, \dot{a}_0, \dot{b}_1, \dot{c}_1) \\
&\quad = -\delta(\dot{c}_1 - \Omega b_1) - \alpha c_1 - \beta f_1^{(s)}
\end{aligned} \tag{23}$$

where for $i = j = l = 1$ Eqs. (10)–(12) gives

$$f_0^{(1)} = 0, \; f_1^{(c)} = \frac{3}{4}b_1^3 + \frac{3}{4}b_1c_1^2, \; f_1^{(s)} = \frac{3}{4}c_1^3 + \frac{3}{4}b_1^2c_1. \tag{24}$$

Thus for $m = k = 1$, Eq. (8) becomes

$$\begin{aligned}
&\ddot{a}_0 = 0, \\
&\ddot{b}_1 + 2\Omega\dot{c}_1 - \Omega^2 b_1 \\
&\quad = -\delta(\dot{b}_1 + \Omega c_1) - \alpha b_1 - \frac{3}{4}\beta b_1\left(b_1^2 + c_1^2\right) \\
&\qquad + Q_0,
\end{aligned} \tag{25}$$

$$\ddot{c}_1 - 2\Omega\dot{b}_1 - \Omega^2 c_1 = -\delta(\dot{c}_1 - \Omega b_1) - \alpha c_1 - \frac{3}{4}\beta c_1\left(c_1^2 + b_1^2\right).$$

The algebraic equations for the traditional harmonic balance with one term is given by the equilibrium point of Eq. (25), i.e.,

$$\begin{aligned} -\Omega^2 b_1^* &= -\delta\Omega c_1^* - \alpha b_1^* - \frac{3}{4}\beta b_1^*\left(b_1^{*2} + c_1^{*2}\right) + Q_0, \\ -\Omega^2 c_1^* &= \delta\Omega b_1^* - \alpha c_1^* - \frac{3}{4}\beta c_1^*\left(b_1^{*2} + c_1^{*2}\right). \end{aligned} \tag{26}$$

Setting $A_1^2 = c_1^{*2} + b_1^{*2}$, and deformation of Eq. (26) produces

$$(\delta\Omega)^2 A_1^2 + A_1^2\left[\left(\alpha - \Omega^2\right) + \frac{3}{4}\beta A_1^2\right]^2 = Q_0^2. \tag{27}$$

From Eq. (27), the first harmonic term amplitude can be determined. Further, from Eq. (26), the coefficient b_1^* and c_1^* are determined. The corresponding stability and bifurcations can be determined from the eigenvalue analysis of the linearized equation of Eq. (25). At the equilibrium point (b_1^*, c_1^*), the linearized equation is

$$\ddot{\mathbf{u}} + \mathbf{C}\dot{\mathbf{u}} + \mathbf{K}\mathbf{u} = \mathbf{0}, \tag{28}$$

where

$$\begin{aligned} &\mathbf{u} = (\Delta b_1, \Delta c_1)^{\mathrm{T}}, \qquad \dot{\mathbf{u}} = (\Delta\dot{b}_1, \Delta\dot{c}_1)^{\mathrm{T}}, \\ &\ddot{\mathbf{u}} = (\Delta\ddot{b}_1, \Delta\ddot{c}_1)^{\mathrm{T}} \\ &\mathbf{C} = \begin{bmatrix} \delta & 2\Omega \\ -2\Omega & \delta \end{bmatrix}, \qquad \mathbf{K} = \begin{bmatrix} K_{11} & K_{12} \\ K_{21} & K_{22} \end{bmatrix}; \\ &K_{11} = \alpha - \Omega^2 + \beta\left(\frac{9}{4}b_1^{*2} + \frac{3}{4}c_1^{*2}\right), \\ &K_{12} = \delta\Omega + \frac{3}{2}\beta b_1^* c_1^*, \\ &K_{21} = -\delta\Omega + \frac{3}{2}\beta b_1^* c_1^*, \\ &K_{22} = \alpha - \Omega^2 + \beta\left(\frac{3}{4}b_1^{*2} + \frac{9}{4}c_1^{*2}\right). \end{aligned} \tag{29}$$

The eigenvalues of the linearized equation is determined by

$$\left|\lambda^2\mathbf{I} + \lambda\mathbf{C} + \mathbf{K}\right| = \mathbf{0}. \tag{30}$$

From the eigenvalues, the stability and bifurcation of approximate symmetric period-1 motion are determined. For one harmonic term, the symmetric period-1 motion cannot be approximated well. Thus, multiple harmonic terms of the Fourier series will be used to predict the symmetric period-1 motions, and then, the asymmetric period-1 motions will be discussed.

The truncated Fourier series solutions will be used to give an approximate solution close to the exact solution. From such approximate, analytical solutions, the equilibrium solution of coefficient dynamical system for the Fourier series of the periodic motion can be obtained from Eq. (20) using the Newton–Raphson method, and the stability and bifurcation analysis of the such equilibrium points can be completed through the eigenvalue analysis. The system parameters are

$$\delta = 0.2, \qquad \alpha = 1.0, \qquad \beta = 4, \qquad Q_0 = 100.0. \tag{31}$$

The backbone curves of harmonic amplitude varying with excitation frequency Ω are illustrated. The harmonic amplitude and phase are defined by

$$\begin{aligned} A_{k/m} &\equiv \sqrt{b_{k/m}^2 + c_{k/m}^2}, \\ \varphi_{k/m} &= \arctan\frac{c_{k/m}}{b_{k/m}} \end{aligned} \tag{32}$$

and the corresponding solution in Eq. (4) is

$$x^*(t) = a_0^{(m)} + \sum_{k=1}^{N} A_{k/m}\cos\left(\frac{k}{m}\Omega t - \varphi_{k/m}\right). \tag{33}$$

For symmetric period-1 motion, the first three harmonic terms of the Fourier series expansion (HB3) will be used to obtain the approximate periodic solutions. The first three harmonic amplitudes (A_k) and phases (φ_k) $(k = 1, 3)$ versus excitation frequency are plotted in Fig. 1(a)–(d), respectively. The solid and dashed curves represent the stable and unstable periodic solutions based on the three terms of the harmonic balance (HB3), respectively. The acronyms

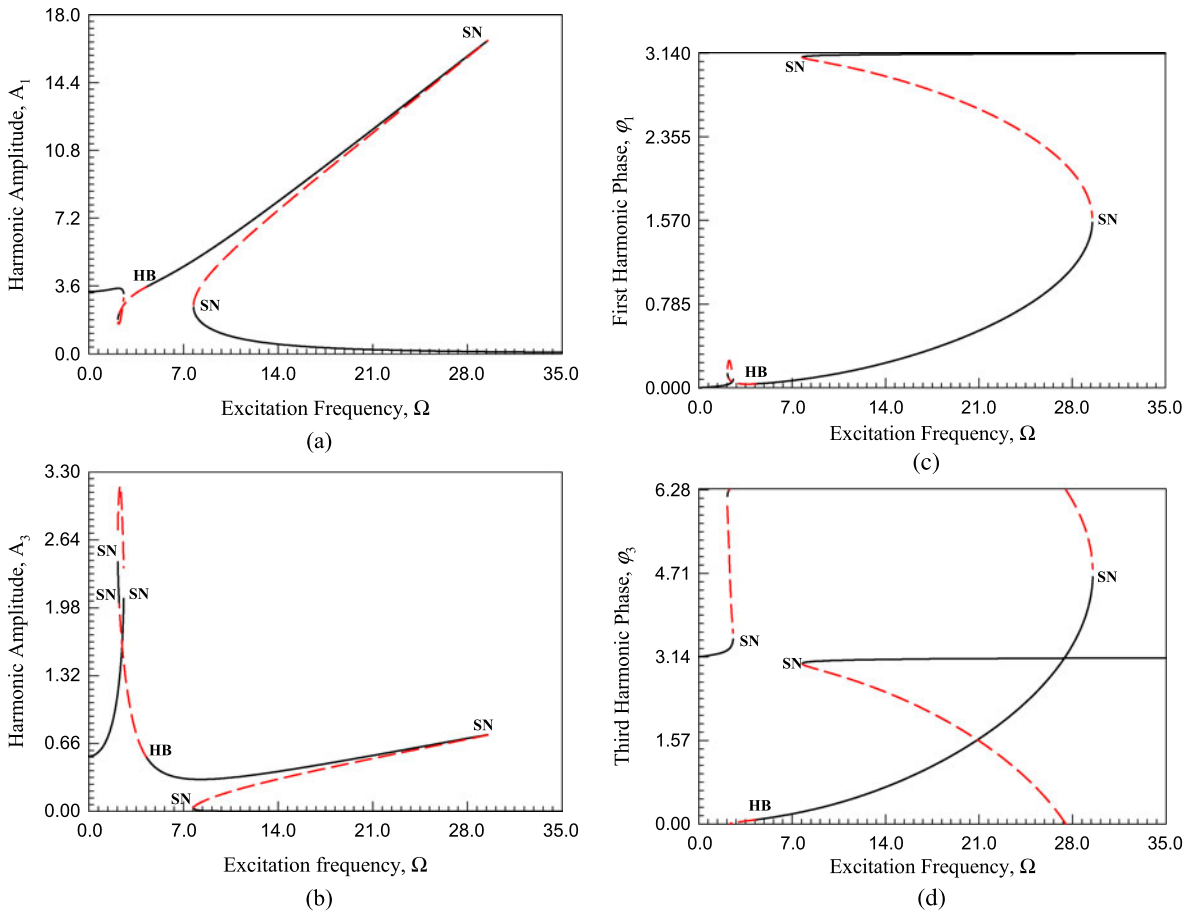

Fig. 1 The analytical prediction of symmetric period-1 solutions based on three harmonic terms (HB3): (**a**) and (**b**) harmonic amplitudes A_k $(k = 1, 3)$; (**c**) and (**d**) harmonic phases φ_k $(k = 1, 3)$. $(\delta = 0.2, \alpha = 1.0, \beta = 4, Q_0 = 100.0)$

"SN" and "HB" represent the saddle-node bifurcation and Hopf bifurcation, respectively. The acronyms "S" and "A" represent the symmetric and asymmetric periodic motions, accordingly. In Fig. 1(a) and (b), the frequency-amplitude curves are presented. For symmetric period-1 motion, $a_0 = A_2 = 0$. From the approximate analysis, the saddle-node bifurcations (SN) occur at $\Omega \approx 2.145, 2.245, 2.575, 7.745, 29.52$. $\Omega = 4.25$ is for Hopf bifurcation. The frequency-amplitude curve (Ω, A_1) in Fig. 1(a) is similar to the one harmonic term. Upper and lower stable branches of solutions exist. The unstable solution is in the middle branch, which is similar to the traditional analysis. The upper branch of symmetric period-1 solution is in $A_1 \in (1.0, 20)$ for $\Omega \in (0, 29.52)$. The lower branch of symmetric period-1 solution is in $A_1 \in (0.0, 2.0)$ for $\Omega \in (7.745, 35)$. From the frequency-amplitude curve (Ω, A_3) in Fig. 1(b), the higher order harmonics contribution to the upper and lower branches are less than 10 % and 1 % for $\Omega > 5$, respectively. However, for $\Omega < 5$, the higher order harmonic contribution to the upper branch solution are the same quantity level. So many higher order harmonic terms should be taken into account. The corresponding phase are presented in Fig. 1(c) and (d). To make illustrations clear, the asymmetric period-1 motion based on the three harmonic terms are presented in Fig. 2(a)–(g). For the asymmetric period-1 motion, $a_0 \neq 0$ and $A_2 \neq 0$. The asymmetric period-1 motion exists in about $\Omega \in (2.24, 4.14)$ and there are four parts of stable motion and four parts of unstable motion. In Fig. 2(a) the constant term coefficient is presented, and the symmetric period-1 motion with $a_0 = 0$ is observed. The eigenvalue anal-

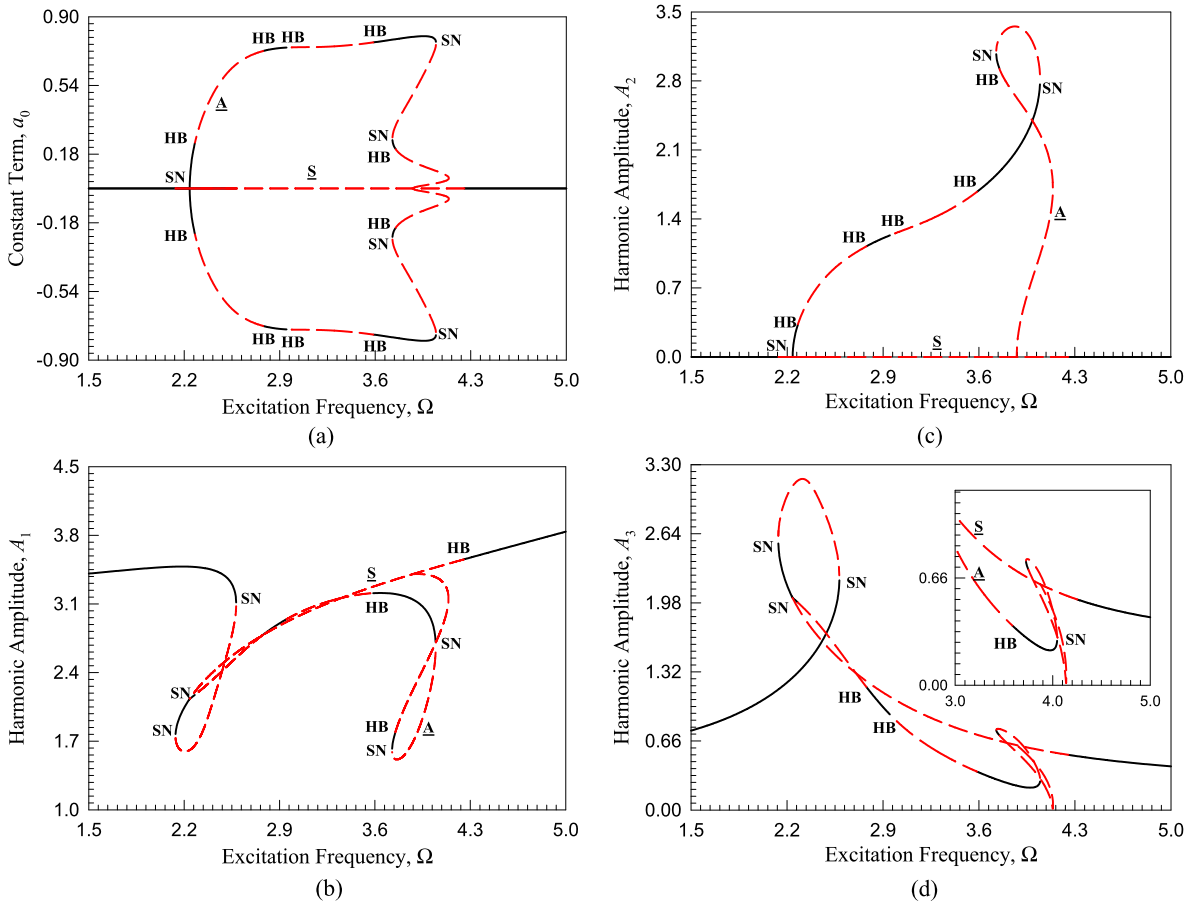

Fig. 2 The analytical prediction of asymmetric period-1 solutions based on three harmonic terms (HB3): (**a**) constant term a_0, (**b**)–(**d**) harmonic amplitudes A_k ($k = 1, 2, 3$); (**e**)–(**g**) harmonic phases φ_k ($k = 1, 3$). ($\delta = 0.2$, $\alpha = 1.0$, $\beta = 4$, $Q_0 = 100.0$)

ysis gives the saddle-node bifurcation (SN) at $\Omega = 2.34, 3.73, 4.05$ and Hopf bifurcation (HB) at $\Omega = 2.28, 2.79, 2.96, 3.61, 3.75$. The saddle-node bifurcations of the symmetric and asymmetric period-1 motion are not the intersected points. In Fig. 2(b), the frequency-amplitude curve (Ω, A_1) for asymmetric period-1 motion is presented. The frequency-amplitude curve (Ω, A_2) for asymmetric period-1 motion is presented in Fig. 2(c) and the symmetric period-1 motion with $A_2 = 0$ is presented as well. The frequency-amplitude curve (Ω, A_3) for asymmetric and symmetric period-1 motion is presented in Fig. 2(d). The phase varying with excitation frequency relative to the first, second and third harmonic terms are presented in Fig. 2(e)–(g). For symmetric motion, the phase is $\varphi_2 = 2\pi$.

Using the three harmonic terms, the parameter map (Ω, Q_0) are presented in Fig. 3 for the period-1 motion, and the corresponding domain are labeled. In the parameter map, the acronyms 'U' and 'S' are for unstable and stable period-1 motions, respectively. $S^m U^n$ means that m stable period-1 motions and n unstable period-1 motions coexist. For $m = 0$, U^n means that n unstable period-1 motions coexist. For $n = 0$, S^m means that m stable period-1 motions coexist. The Hopf bifurcation boundaries (HB) are given by dashed curves. The saddle-node bifurcation boundaries (SN) are given by solid curves. The dash-dot curves give the saddle switching. In Fig. 3(a), the global view of parameter map is given and the zoomed view of the local details is presented in Fig. 3(b) and (c). Again the parameter map for the lower excitation frequency region may not be accurate, and a more comprehensive investigation should be completed.

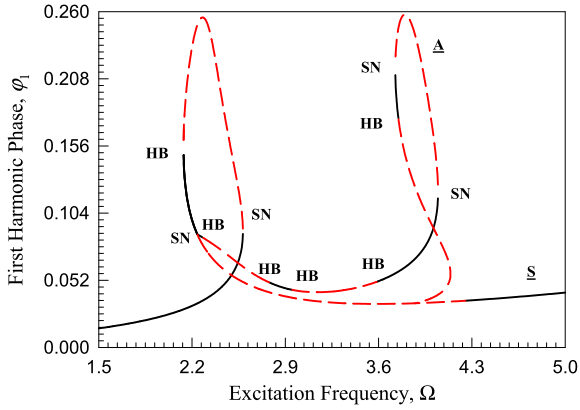

(e)

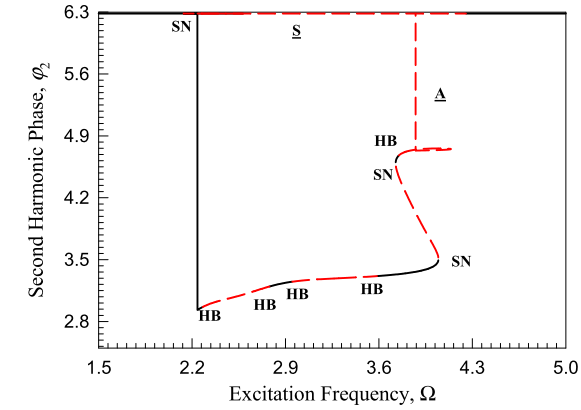

(f)

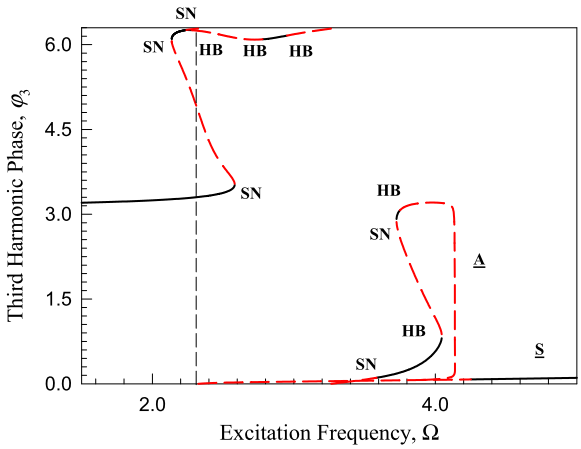

(g)

Fig. 2 (*Continued*)

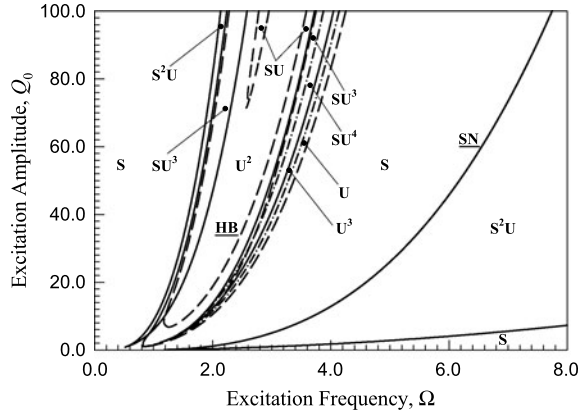

(a)

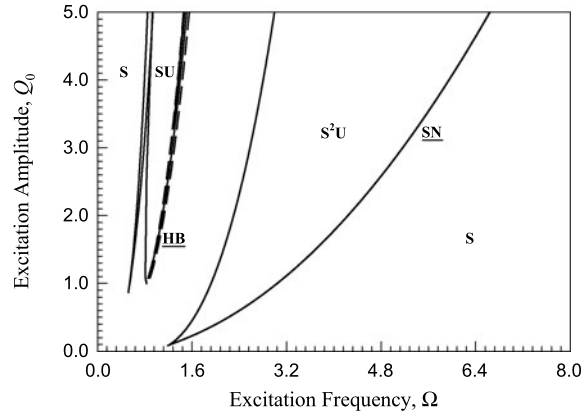

(b)

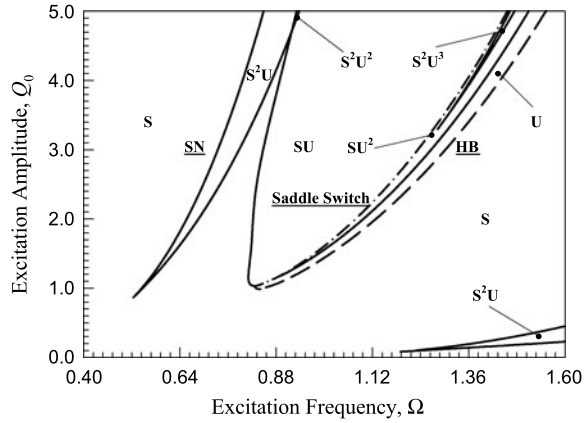

(c)

Fig. 3 A parameter map from the analytical prediction of periodic solutions based on three harmonic terms (HB3): (**a**) Global view and (**b**) zoomed view. ($\delta = 0.2$, $\alpha = 1.0$, $\beta = 4.0$)

To obtain the appropriate analytical solution for period-1 motion, the ten harmonic terms are used to give the period-1 motions. The symmetric and asymmetric period-1 motions are presented in Fig. 4(i)–(xx). In Fig. 4(i) and (ii), global and zoomed views for constant term coefficients varying with excitation frequency are presented. The asymmetric period-1 mo-

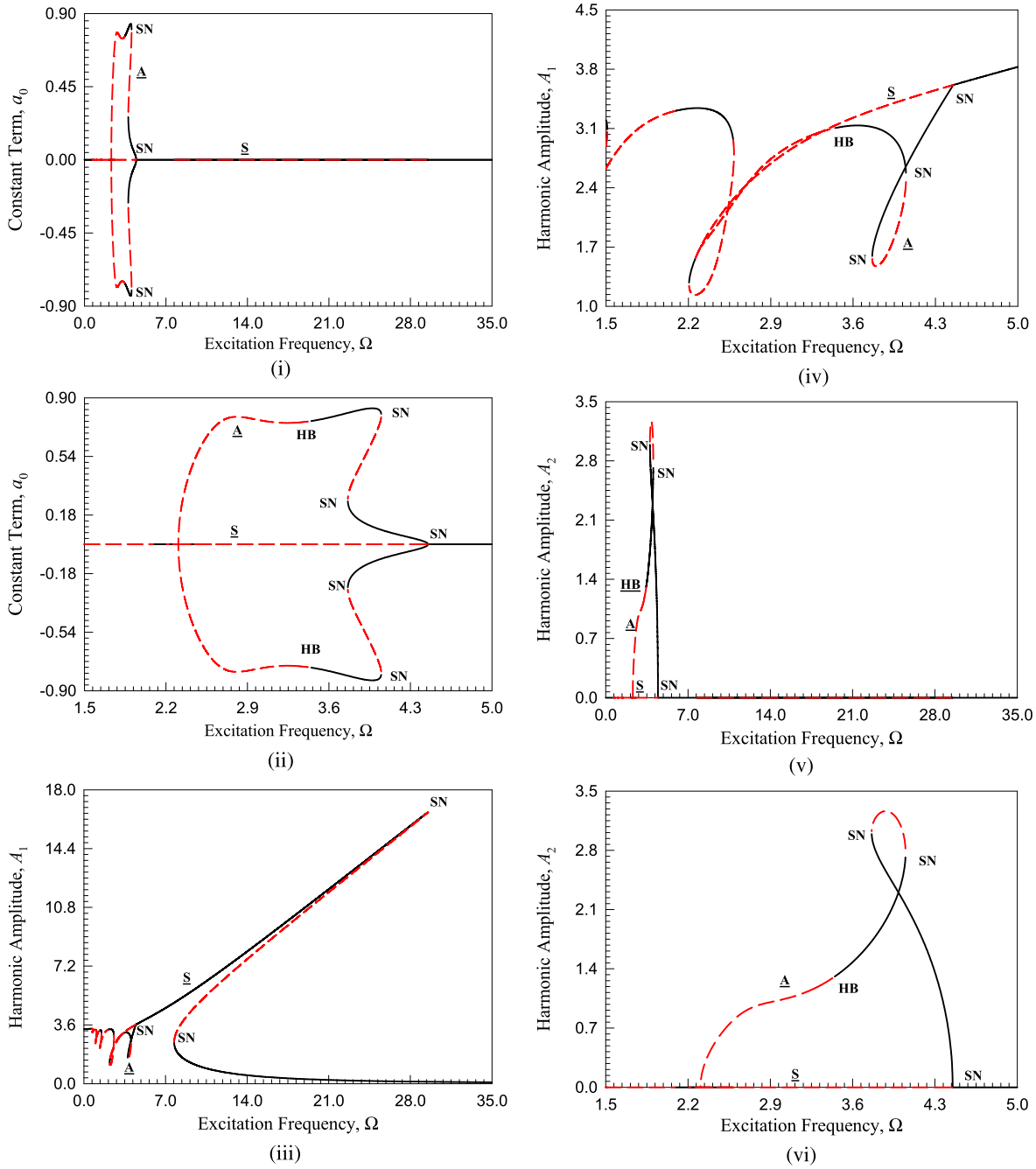

Fig. 4 The analytical prediction of asymmetric period-1 solutions based on ten harmonic terms (HB10): (**i**) and (**ii**) constant term a_0 and zoomed view, (**iii**)–(**xxii**) harmonic amplitudes and zoomed views A_k ($k = 1, 2, \ldots, 10$). ($\delta = 0.2$, $\alpha = 1.0$, $\beta = 4$, $Q_0 = 100.0$)

tion exists in $\Omega \in (2.306, 4.354)$ different from $\Omega \in (2.24, 4.14)$ given by the three harmonic terms. The stability ranges and bifurcation points are different because the approximate, period-1 solution with three harmonic terms cannot provide the accurate period-1 solutions for $\Omega < 5$. For the asymmetric period-1 motion, the range of excitation frequency is in an interval of $\Omega \in (2.0, 5.0)$. In Fig. 4(iii) and (iv), the frequency-amplitude curves (Ω, A_1) for period-1 motions are presented. The solutions of symmetric period-1motion

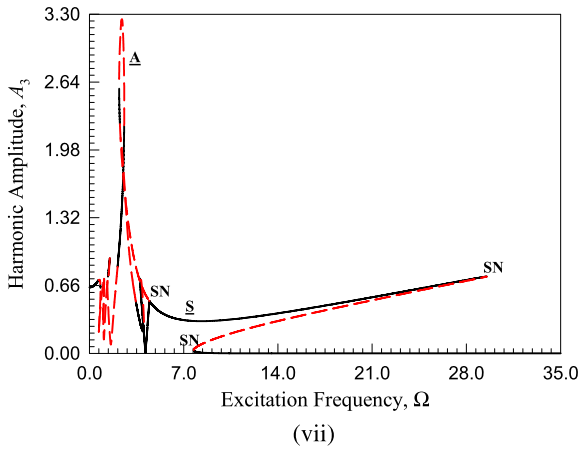

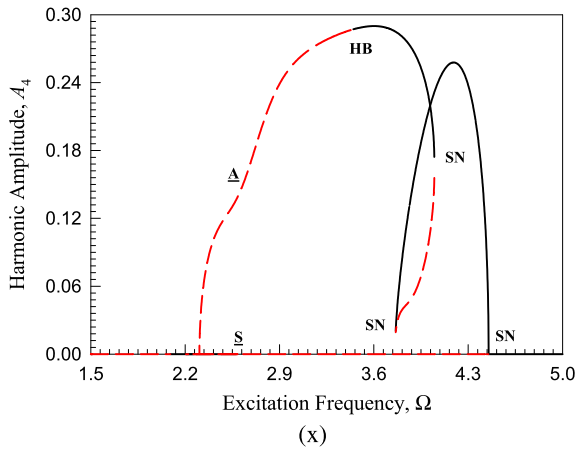

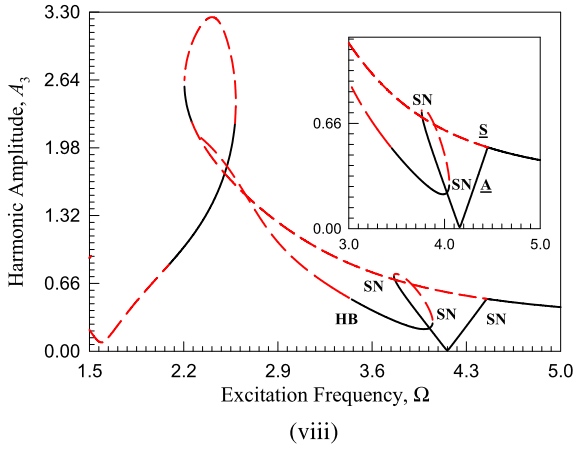

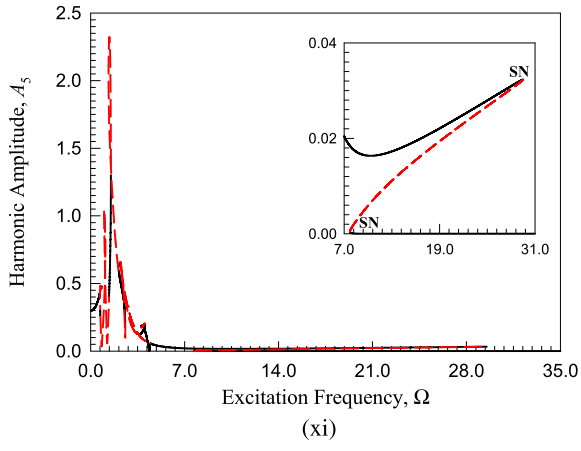

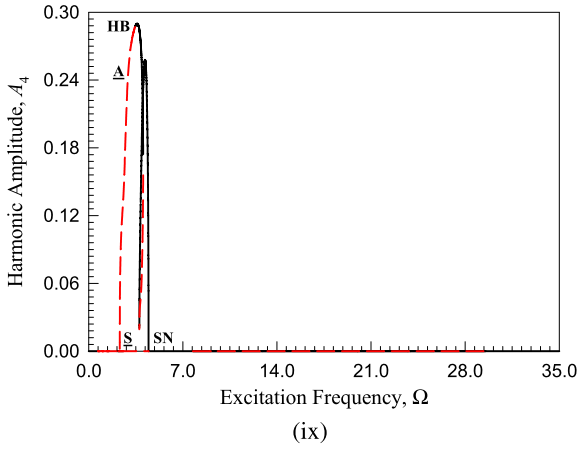

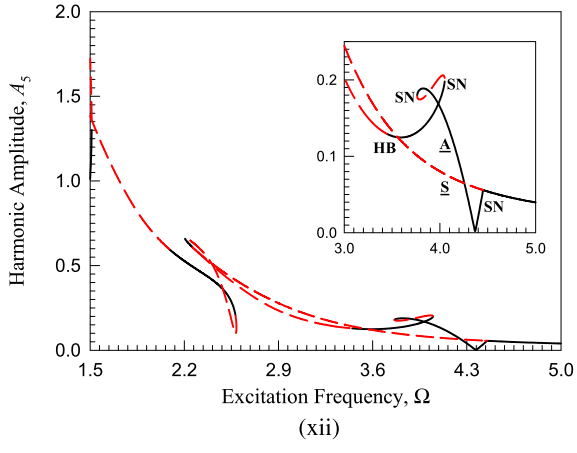

Fig. 4 (*Continued*)

given by the ten harmonic terms are almost the same as by the three harmonic terms for $\Omega > 5$. However, for $\Omega < 5$, the solutions based on the three and ten harmonic terms are different because the higher order harmonic terms have significant contributions on the solutions. In Fig. 4(v) and (vi), the frequency-amplitude curves (Ω, A_2) for asymmetric period-1 motions are presented because of $A_2 = 0$ for this symmetric period-1 motion. Comparing this ten harmonic term solution with the three harmonic term so-

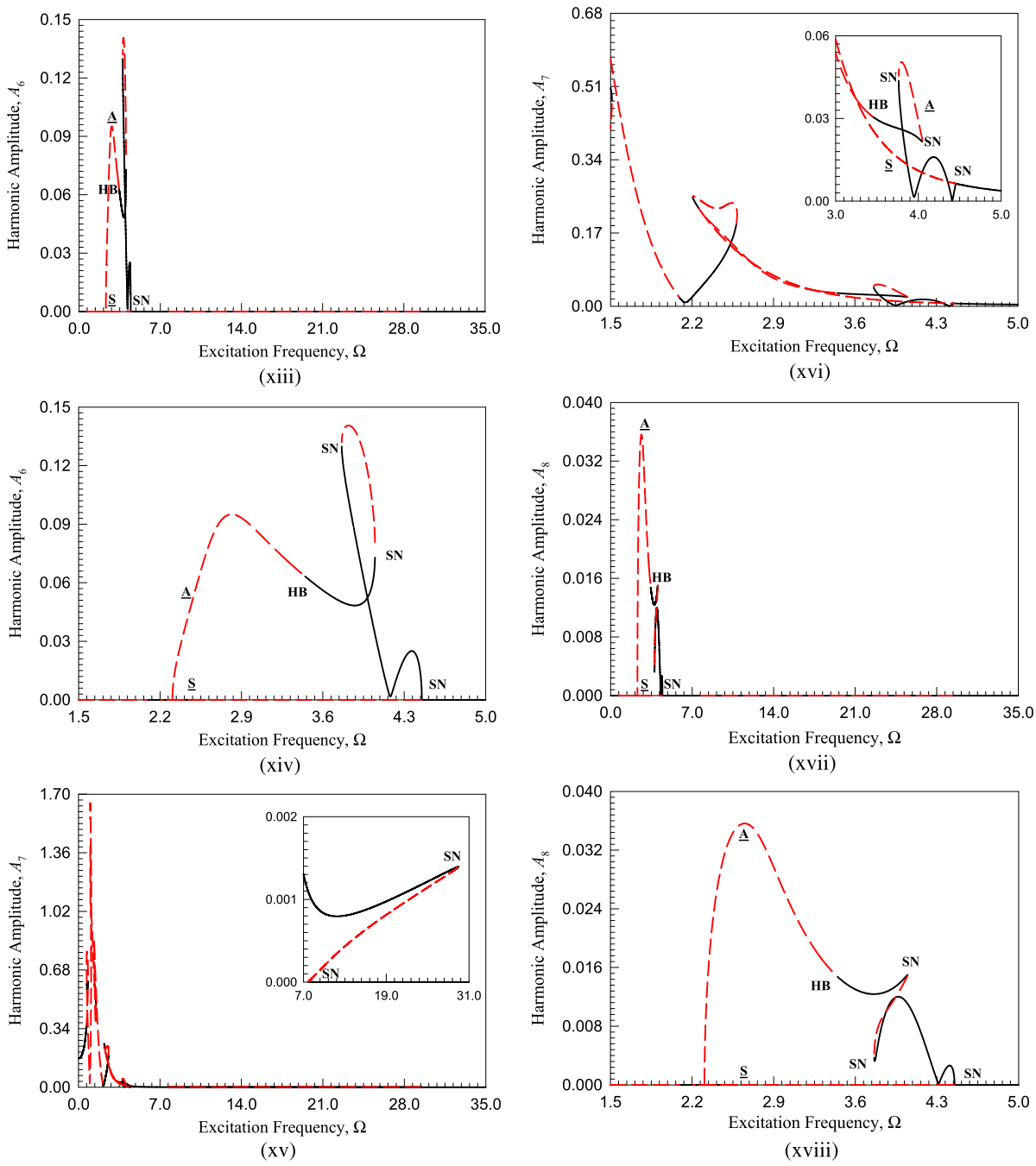

Fig. 4 (*Continued*)

lution, the frequency-amplitude curves for asymmetric period-1 motion are modified with $a_0, A_2 \sim 10^0$ for $\Omega \in (1.5, 5.0)$. In Fig. 4(vii) and (viii), the frequency-amplitude curves (Ω, A_3) for symmetric and asymmetric period-1 motions are presented. The amplitude A_3 based on the ten and three harmonic terms are almost same for $\Omega > 5$. However, for $\Omega < 5$, the symmetric and asymmetric response amplitudes for symmetric and asymmetric period-1 motion are quite different because the higher order harmonic terms pos-

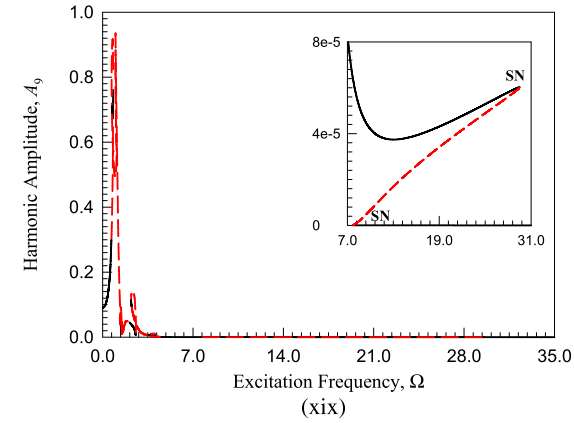

(xix)

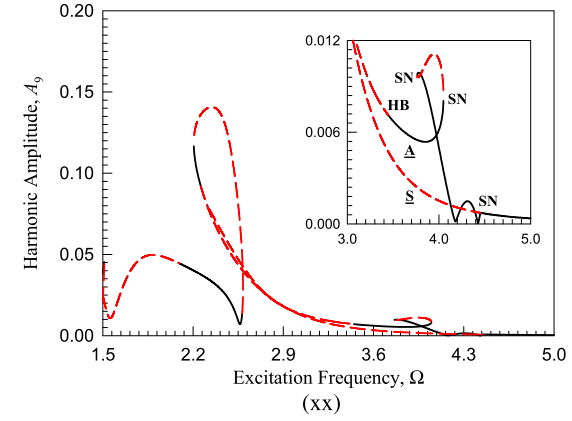

(xx)

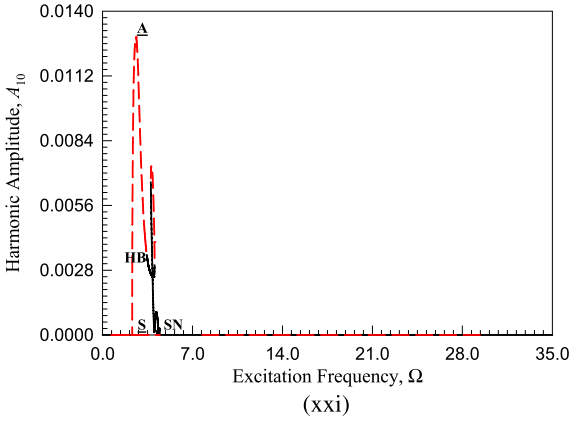

(xxi)

Fig. 4 (*Continued*)

sess more effects on the period-1 motion solutions. For asymmetric motion, $A_4 \sim 10^{-1}$, and $A_m \sim 10^1$ $(m = 1, 2, 3, 5)$, as shown in Fig. 4(ix)–(xii). From Fig. 4(xiii)–(xxii), we have $A_m \sim 10^{-2}$ $(m = 6, 8, 10)$ and $A_{7,9} \sim 10^{-1}$ for $\Omega < 5$. However, for $\Omega > 5$, we have $A_5 \leq 0.04$, $A_7 \leq 0.002$ and $A_9 \leq 10^{-4}$. Thus, for symmetric period-1 motion, the Fourier series solution with three harmonic terms can give a good approxima-

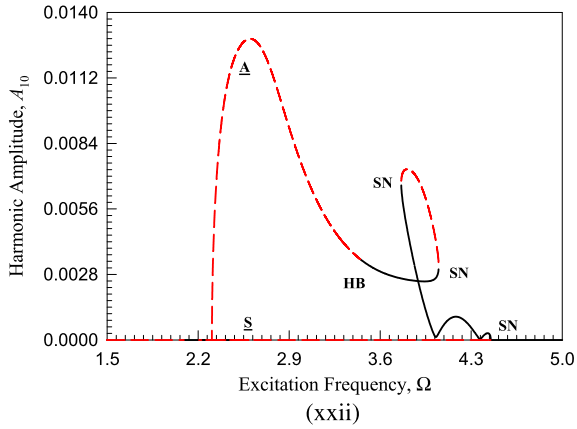

(xxii)

Fig. 4 (*Continued*)

tion for $\Omega > 5$. From the quantity level of harmonic response amplitudes, effects of the corresponding harmonic terms on the solutions can be observed.

Based on the Fourier solution of period-1 motion with the ten harmonic terms, the asymmetric period-1 motion has a Hopf bifurcation. Thus a period-2 motion will be formed from such asymmetric period-1 motion. The Fourier series expression for period-2 motion needs 20 harmonic terms. Once this period-2 motion has a Hopf bifurcation, the period-4 motion will appear. Further, the Fourier series solution with 40 harmonic terms will be used to describe the period-4 motion. The analytical route of an asymmetric period-1 motion to period-4 motions $(m = 4)$ is presented in Fig. 5(i)–(xxiv) through the constant terms $(a_0^{(m)})$ for the left and right sides of the symmetric motion and the harmonic amplitude $A_{k/m}$ $(k = 1, 2, \ldots, 12)$, $A_{k/m}$ $(k = 16, 20, \ldots, 36)$ and $A_{k/m}$ $(k = 37, 38, 39, 40)$. From the asymmetric period-1 motion, at $\Omega \approx 3.447$, the approximate solution for asymmetric period-2 motions is obtained. From the asymmetric period-2 motion, at $\Omega \approx 3.321$, the approximate solution for asymmetric period-4 motions is obtained. From the asymmetric period-4 motion, at $\Omega \approx 3.306$, the approximate solutions for asymmetric period-8 motion can be obtained similarly. Continuously, the chaotic motions for such hardening Duffing oscillator can be achieved. $a_0^{(m)} \sim 1$ for $\Omega \in (3.0, 3.5)$. In Fig. 5(iii), the subharmonic amplitude $A_{1/4} \sim 10^{-1}$ for period-4 motion is presented and $A_{1/4} = 0$ for period-2 and period-1 motions. In Fig. 5(iv), the subharmonic amplitude $A_{1/2} \sim 10^{-1}$ for period-2 and period-4 motions are presented and $A_{1/2} = 0$ for period-1 motion. In Fig. 5(v), the

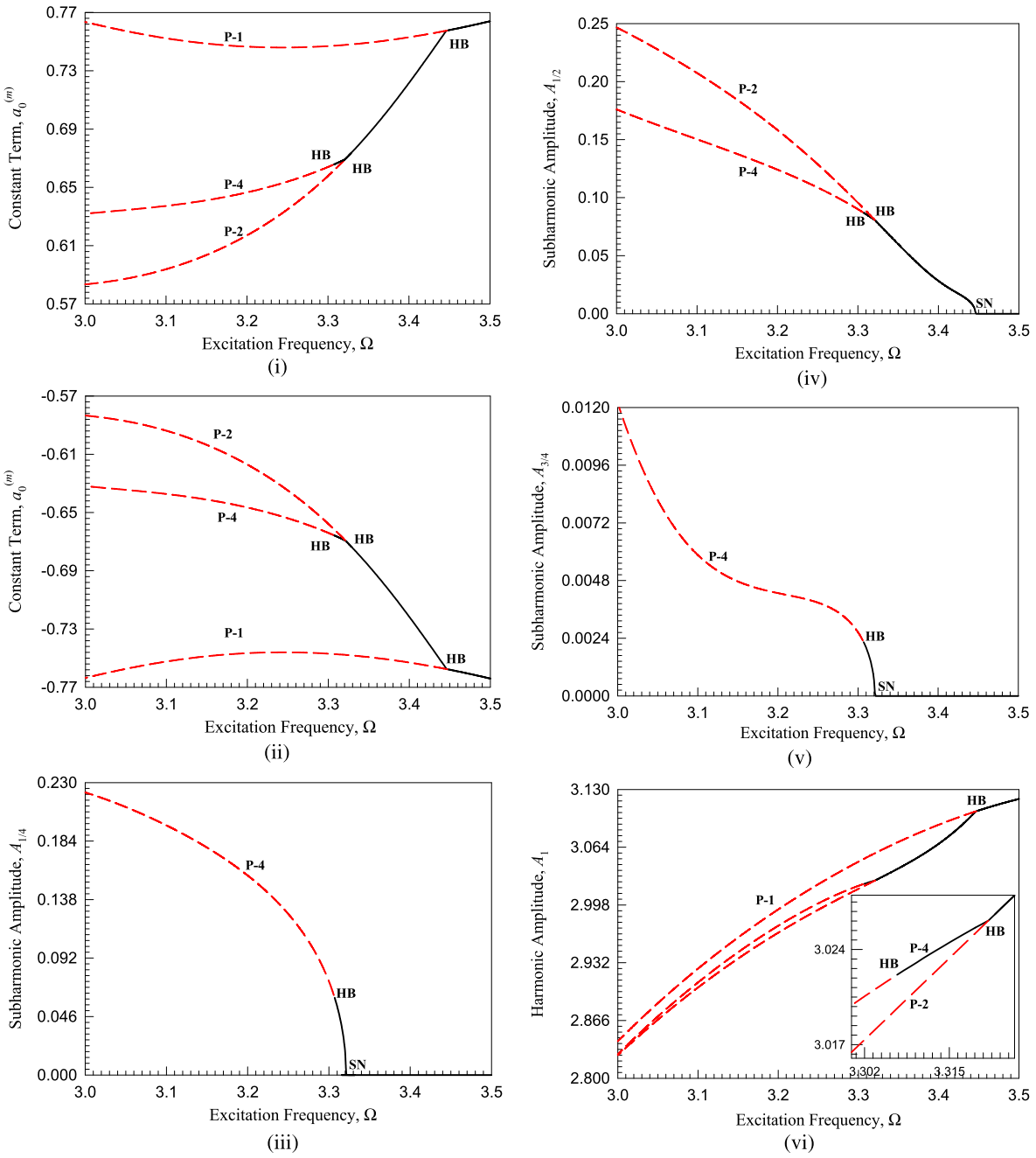

Fig. 5 The analytical routes of asymmetric period-1 motion to chaos based on 40 harmonic terms (HB40): (**i**) and (**ii**) constant term $a_0^{(m)}$, (**iii**)–(**xiv**) harmonic amplitudes $A_{k/m}$ ($k = 1, 2, \ldots, 12,\ m = 4$), (**xv**)–(**xx**) harmonic amplitudes $A_{k/m}$ ($k = 16, 20, \ldots, 36, m = 4$), (**xxi**)–(**xxxiv**) harmonic amplitudes $A_{k/m}$ ($k = 37, 38, 39, 40,\ m = 4$). ($\delta = 0.2,\ \alpha = 1.0,\ \beta = 4,\ Q_0 = 100.0$)

subharmonic amplitude $A_{3/4} \sim 10^{-2}$ for period-4 motion is presented and $A_{3/4} = 0$ for period-2 and period-1 motions. In Fig. 5(vi), the harmonic amplitude A_1 for period-1, period-2, period-4 motions are presented and $A_1 \in (2.8, 3.13)$ for $\Omega \in (3.0, 3.5)$. In Fig. 5(vii), the subharmonic amplitude $A_{5/4} \sim 10^{-2}$ for period-

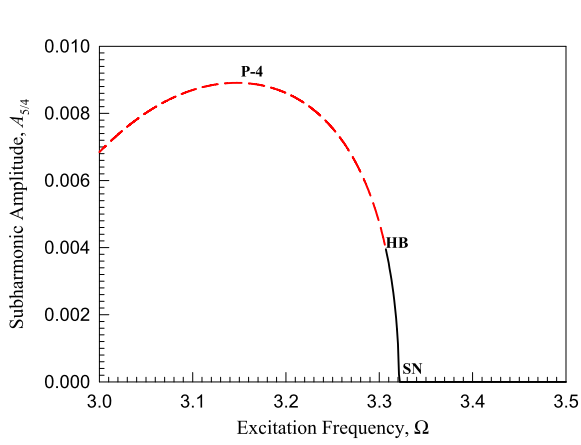

(vii)

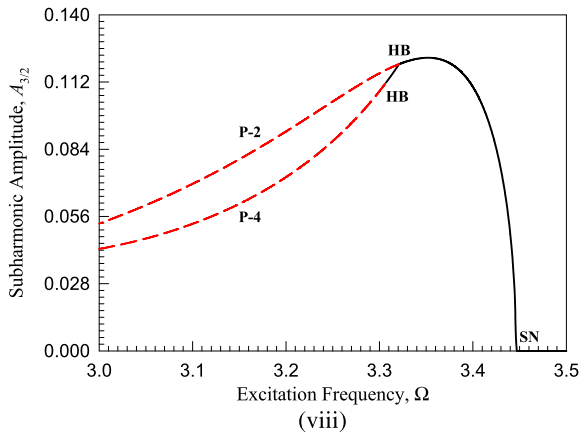

(viii)

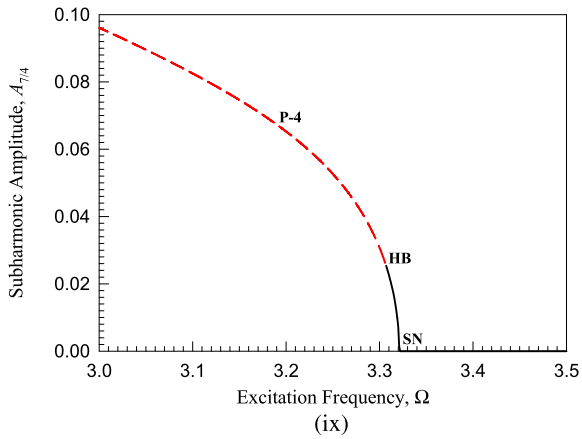

(ix)

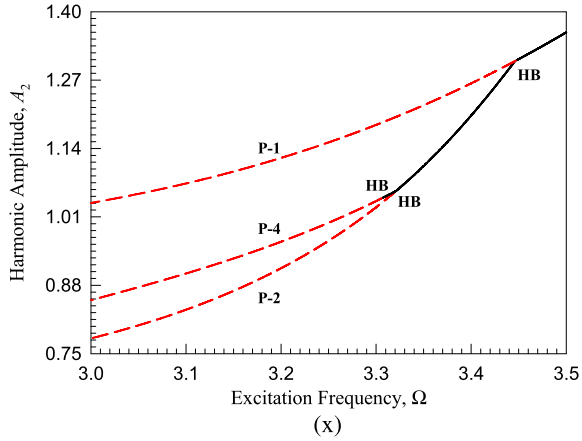

(x)

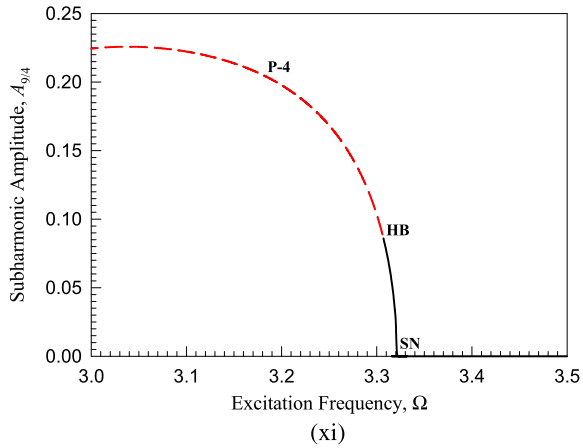

(xi)

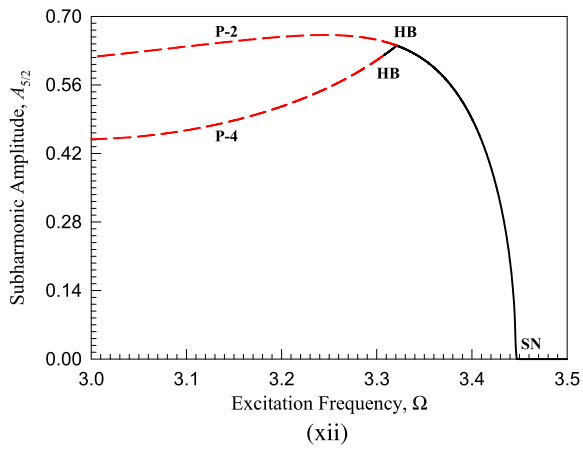

(xii)

Fig. 5 (*Continued*)

4 motion is presented and $A_{5/4} = 0$ for period-2 and period-1 motions. In Fig. 5(viii), the subharmonic amplitude $A_{3/2} \sim 10^{-1}$ for period-2 and period-4 motions are presented and $A_{3/2} = 0$ for period-1 motion. In Fig. 5(ix), the subharmonic amplitude $A_{7/4} \sim 10^{-1}$ for period-4 motion is presented and $A_{7/4} = 0$ for period-2 and period-1 motions. In Fig. 5(x), the harmonic amplitude A_2 for period-1, period-2, period-4 motions are presented and $A_2 \in (0.75, 1.40)$ for $\Omega \in (3.0, 3.5)$. In Fig. 5(xi), the subharmonic ampli-

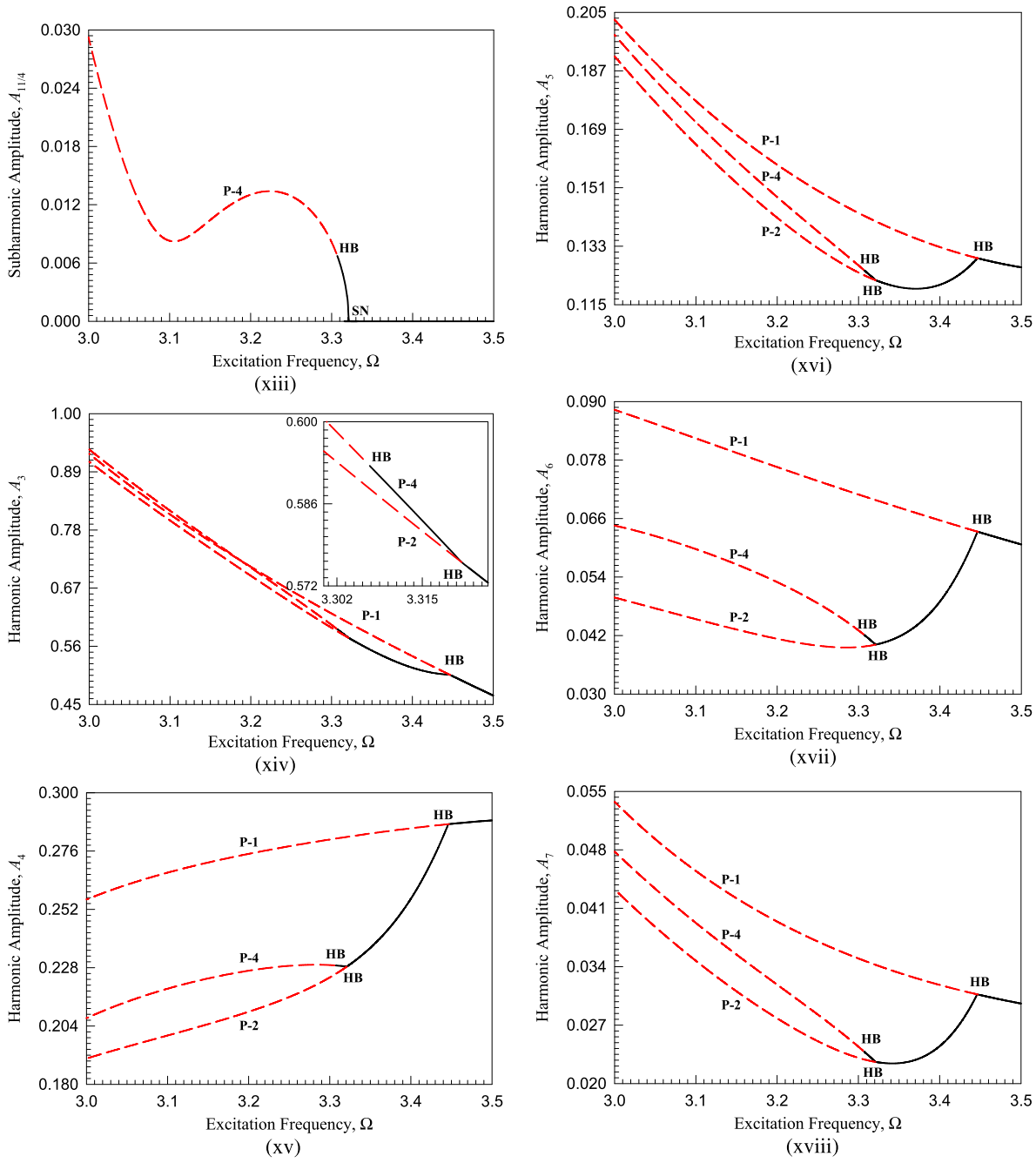

Fig. 5 (*Continued*)

tude ($A_{9/4} \sim 10^{-1}$) for period-4 motion is presented and $A_{9/4} = 0$ for period-2 and period-1 motions. In Fig. 5(xii), the subharmonic amplitude $A_{5/2} \sim 10^{0}$ for period-2 and period-4 motions are presented and $A_{5/2} = 0$ for period-1 motion. In Fig. 5(xiii), the subharmonic amplitude ($A_{11/4} \sim 10^{-2}$) for period-4 motion is presented and $A_{11/4} = 0$ for period-2 and period-1 motions. In Fig. 5(xiv), the harmonic amplitude A_3 for period-1, period-2 and period-4 motions are presented and $A_3 \in (0.45, 1.0)$ for $\Omega \in (3.0, 3.5)$.

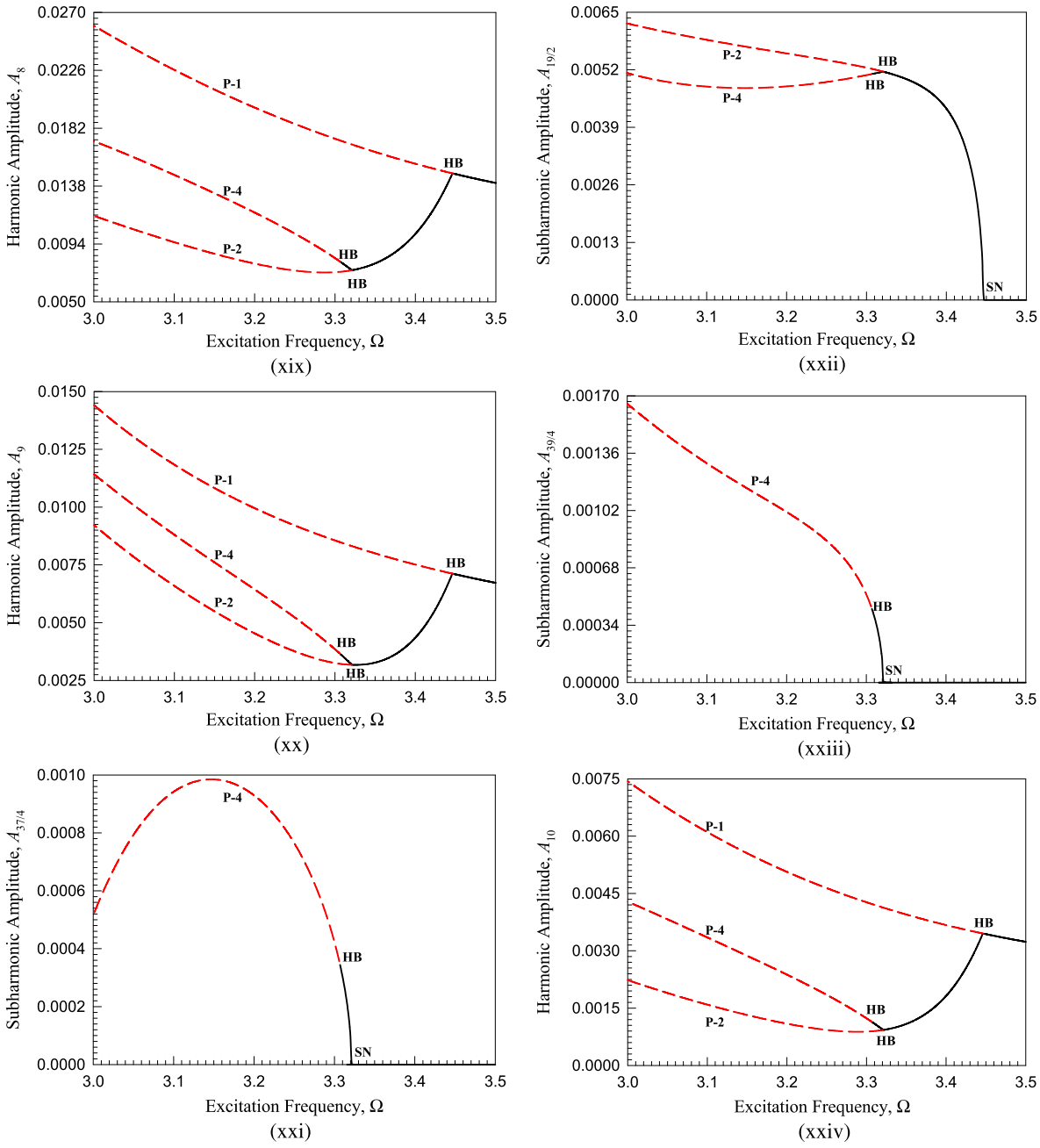

Fig. 5 (*Continued*)

Due to limitation of the number of pages, only harmonic terms $A_{k/m}$ $(m = 4, k = 16, 20, \ldots, 36)$ are presented in Fig. 5(xvi)–(xx) or period-1, period-2, and period-4 motions. $A_{4,5,6} \sim 10^{-1}$ and $A_{7,8,9} \sim 10^{-2}$. To show convergence, in Fig. 5(xxi), the subharmonic amplitude ($A_{37/4} \sim 10^{-3}$) for period-4 motion is presented and $A_{37/4} = 0$ for period-2 and period-1 motions. In Fig. 5(xxii), the subharmonic amplitude $A_{19/2} \sim 10^{-3}$ for period-2 and period-4 motions are presented and $A_{19/2} = 0$ for period-1 motion. In Fig. 5(xxiii), the subharmonic amplitude ($A_{39/4} \sim 10^{-3}$) for period-4 motion is pre-

sented and $A_{39/4} = 0$ for period-2 and period-1 motions. In Fig. 5(xxiv), the harmonic amplitude A_{10} for period-1, period-2 and period-4 motions are presented and $A_{10} \in (0.0015, 0.0075)$ for $\Omega \in (3.0, 3.5)$. The harmonic phases for right and left asymmetry have a relation like $\varphi^L_{k/m} = \text{mod}(\varphi^R_{k/m} + (k/m + 1)\pi, 2\pi)$, which is not presented because of limitation of the number of pages.

4 Numerical illustrations

In this section, the initial conditions for numerical simulations are computed from approximate analytical solutions of periodic solutions. In all plots, circular symbols gives approximate solutions, and solid curves give numerical simulation results. The acronym "I.C." with a large circular symbol represents initial condition for all plots. The numerical solutions of periodic motions are generated via the symplectic scheme.

The displacement and trajectory in phase plane for the approximate solutions of stable and unstable symmetric period-1 motion are illustrated in Fig. 6(a)–(f). In addition, the numerical simulations are superimposed, and the initial conditions are obtained from the approximate solutions of period-1 motion. The analytical solution of period-1 motion is given by the Fourier series with the ten harmonic terms (HB10). For the upper branch of stable symmetric period-1 motion, the initial conditions are $t_0 = 0.0$, $x_0 \approx 6.296950$ and $y_0 \approx 11.422100$ for $\Omega = 10$ with other parameters in Eq. (31). For the lower branch of stable symmetric period-1 motion with same parameters, the initial conditions are $t_0 = 0.0$, $x_0 \approx -1.045500$, and $y_0 \approx 0.220845$ for $\Omega = 10$. For the middle branch of unstable symmetric period-1 motion with same parameters, the initial conditions are $t_0 = 0.0$, $x_0 \approx -5.192940$, and $y_0 \approx 6.918470$ for $\Omega = 10$.

In Fig. 6(a) and (b), the analytical and numerical solutions overlap each other for the displacement and trajectory of the symmetric period-1 motion. The symmetry of displacement is observed. For 40 periods, the analytical and numerical trajectories of the symmetric period-1 motion in phase plane are plotted and both analytical and numerical results match very well. The motion for one period is labeled. The analytical and numerical solutions for the displacement of the symmetric period-1 motion on the lower branch are presented in Fig. 6(c) and (d), respectively. The analytical and numerical results are in good agreement. For the unstable symmetric period-1 motion, the numerical and analytical displacement and trajectory are presented in Fig. 6(e) and (f), respectively. For the first few periods, analytical and numerical unstable period-1 motions match very well. However, after a few periods, the numerical unstable period-1 motion moves away and arrives at a new periodic motion. Such a new stable periodic motion is symmetric period-3 motion, which will be discussed in sequel.

In this paper, asymmetric periodic motion is of great interest. The displacement, velocity and trajectory in phase plane will be illustrated. Taking account of $\Omega = 4.1$, a stable asymmetric motion and an unstable symmetric motion coexist. For the stable asymmetric period-1 motion, the initial condition is $t_0 = 0.0$, $x_0 \approx 2.735740$, and $y_0 \approx -19.407900$. For the unstable symmetric period-1 motion, the initial condition is $t_0 = 0.0$, $x_0 \approx 4.137450$, and $y_0 \approx 1.295130$. Numerical and analytical solutions match very well. After 40 excitation periods, the numerical and analytical solutions of the stable asymmetric period-1 motion perfectly match as shown in Fig. 7. Compared to the unstable symmetric period-1 motion in Fig. 6(e) and (f), this unstable symmetric period-1 motion possesses a different trajectory shape and its numerical solutions moves away to a stable asymmetric period-1 motion.

In Fig. 8, the unstable asymmetric period-1 motions and the stable asymmetric period-2 motions are presented for $\Omega = 3.4$. The initial conditions are $t_0 = 0.0$, $x_0 \approx 2.936730$, and $y_0 \approx -1.173750$ (unstable period-1 motion) and $t_0 = 0.0$, $x_0 \approx 3.358240$, and $y_0 \approx -1.225180$ (stable period-2 motion). In Fig. 8(a)–(c), displacement, velocity and trajectory for the unstable asymmetric period-1 motions are presented. The unstable asymmetric period-1 motion moves to the stable asymmetric period-2 motion. The analytical solution of the unstable period-1 motion is given by the Fourier series solution with 10 harmonic terms. For the stable asymmetric period-2 motion, the corresponding analytical solution is given by the Fourier series solution with 20 harmonic terms, and the analytical and numerical solutions of displacement, velocity and trajectories are presented in Fig. 8(d)–(f), respectively. For the further demonstration of the analytical tree of periodic motions from asymmetric period-1 motion, consider an excitation frequency of $\Omega = 3.32$ for which the unstable period-1, unstable period-2 and stable period-4 motions coexist on the analytical bifurcation tree from the asym-

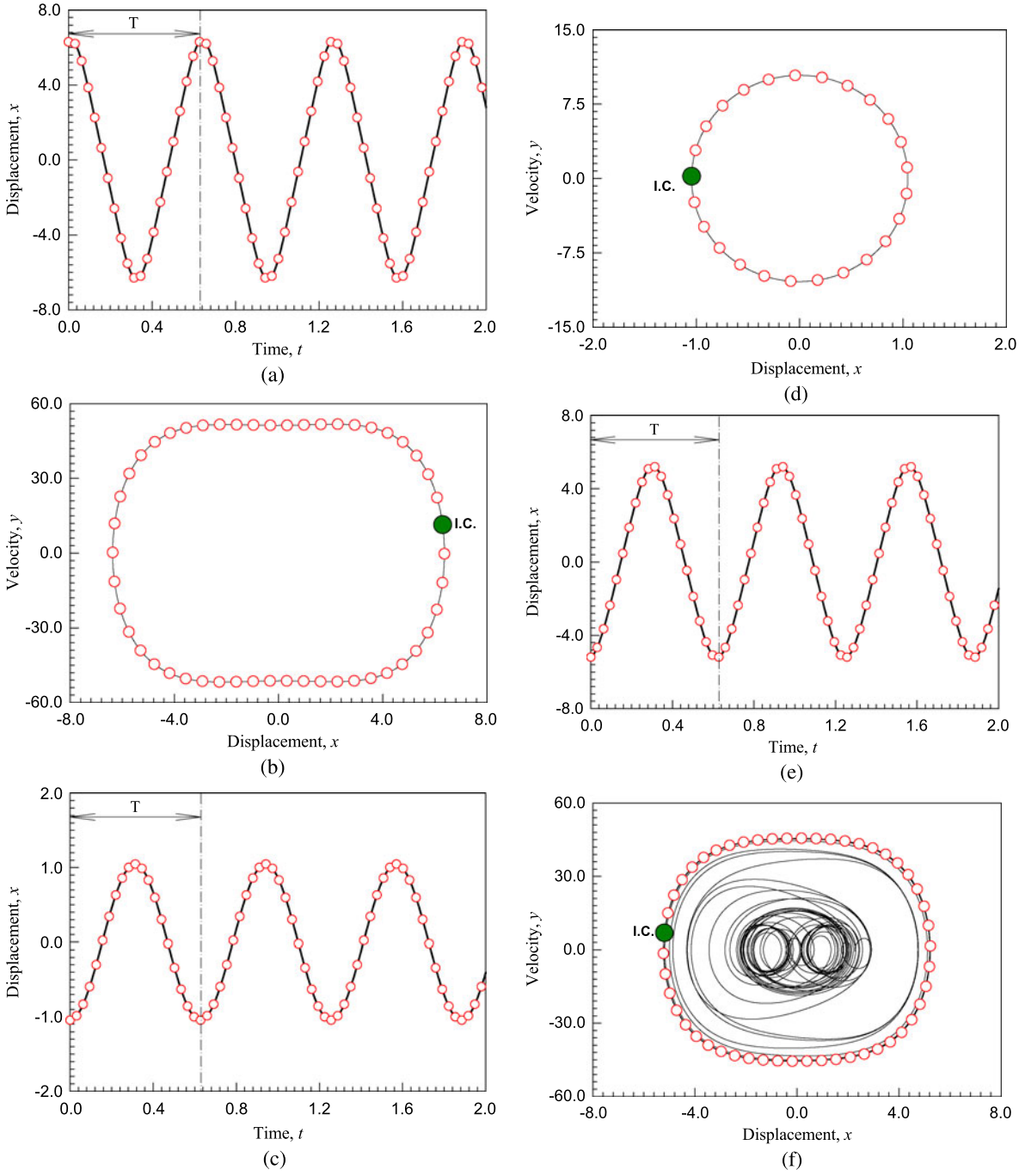

Fig. 6 A stable, symmetric period-1 motions (HB10) (upper branch): (**a**) displacement and (**b**) phase plane ($x_0 \approx 6.296950$, $y_0 \approx 11.422100$). A stable, symmetric period-1 motion (HB10) (lower branch): (**c**) displacement and (**d**) phase plane ($x_0 \approx -1.045500$, $y_0 \approx 0.220845$). An unstable, symmetric period-1 motion (HB10) (*middle branch*): (**e**) displacement and (**f**) phase plane ($x_0 \approx -5.192940$, $y_0 \approx 6.918470$). ($\Omega = 10$, $\delta = 0.2$, $\alpha = 1.0$, $\beta = 4$, $Q_0 = 100.0$)

metric period-1 motion. The displacements and trajectories for three periodic motions are presented in Fig. 9(a)–(f). The analytical solutions for period-1, period-2 and period-4 motions are expressed by the

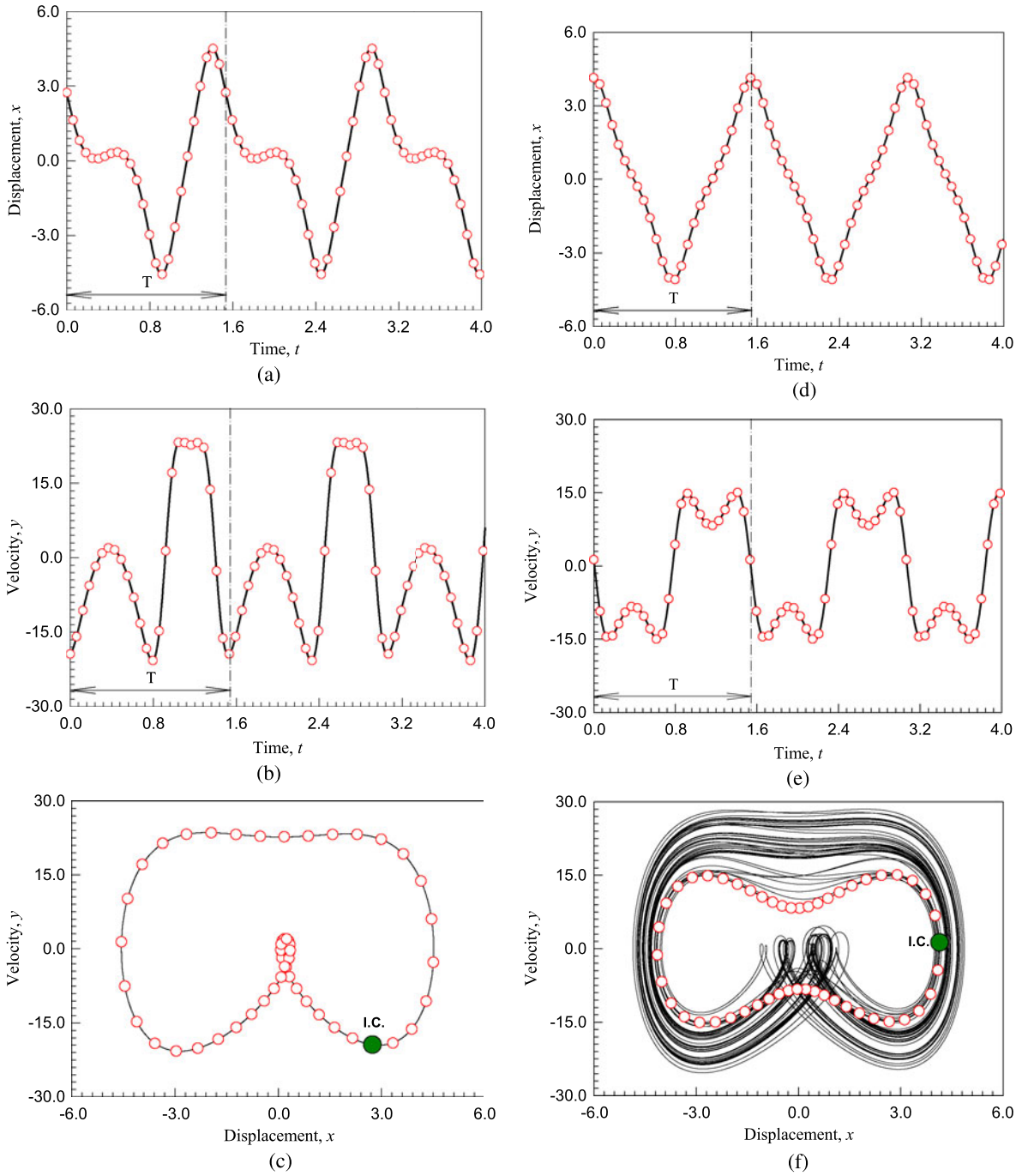

Fig. 7 A stable, asymmetric period-1 motions (HB10): (**a**) displacement, (**b**) velocity and (**c**) phase plane ($x_0 \approx 2.735740$, $y_0 \approx -19.407900$). An unstable, asymmetric period-1 motion (HB10): (**d**) displacement, (**e**) velocity and (**f**) phase plane ($x_0 \approx 4.960370$, $y_0 \approx 3.734470$). ($\Omega = 4.1$, $\delta = 0.2$, $\alpha = 1.0$, $\beta = 4$, $Q_0 = 100.0$)

Fourier series with 10, 20 and 40 harmonic terms. The numerical solutions for the unstable period-1 and unstable period-2 motions go away from the corresponding analytical solutions to the stable period-4 motion. However, the analytical and numerical solutions for period-4 motions match very well.

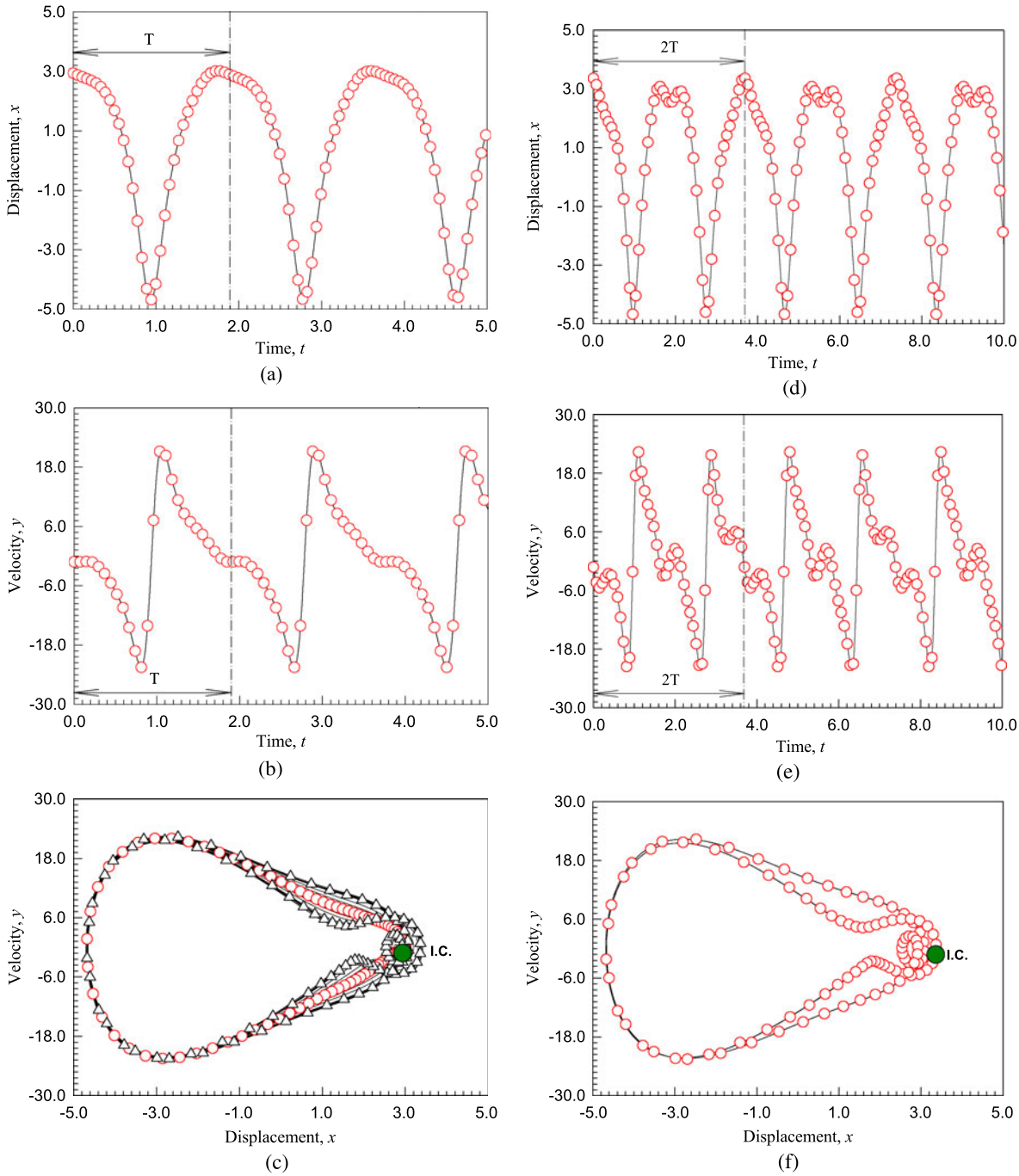

Fig. 8 An unstable, asymmetric period-1 motions (HB10): (**a**) displacement, (**b**) velocity, and (**c**) phase plane ($x_0 \approx 2.936730$, $y_0 \approx -1.173750$). A stable asymmetric period-2 motion (HB20): (**d**) displacement, (**e**) velocity, and (**f**) phase plane ($x_0 \approx 3.358240$, $y_0 \approx -1.225180$). ($\Omega = 3.4$, $\delta = 0.2$, $\alpha = 1.0$, $\beta = 4$, $Q_0 = 100.0$)

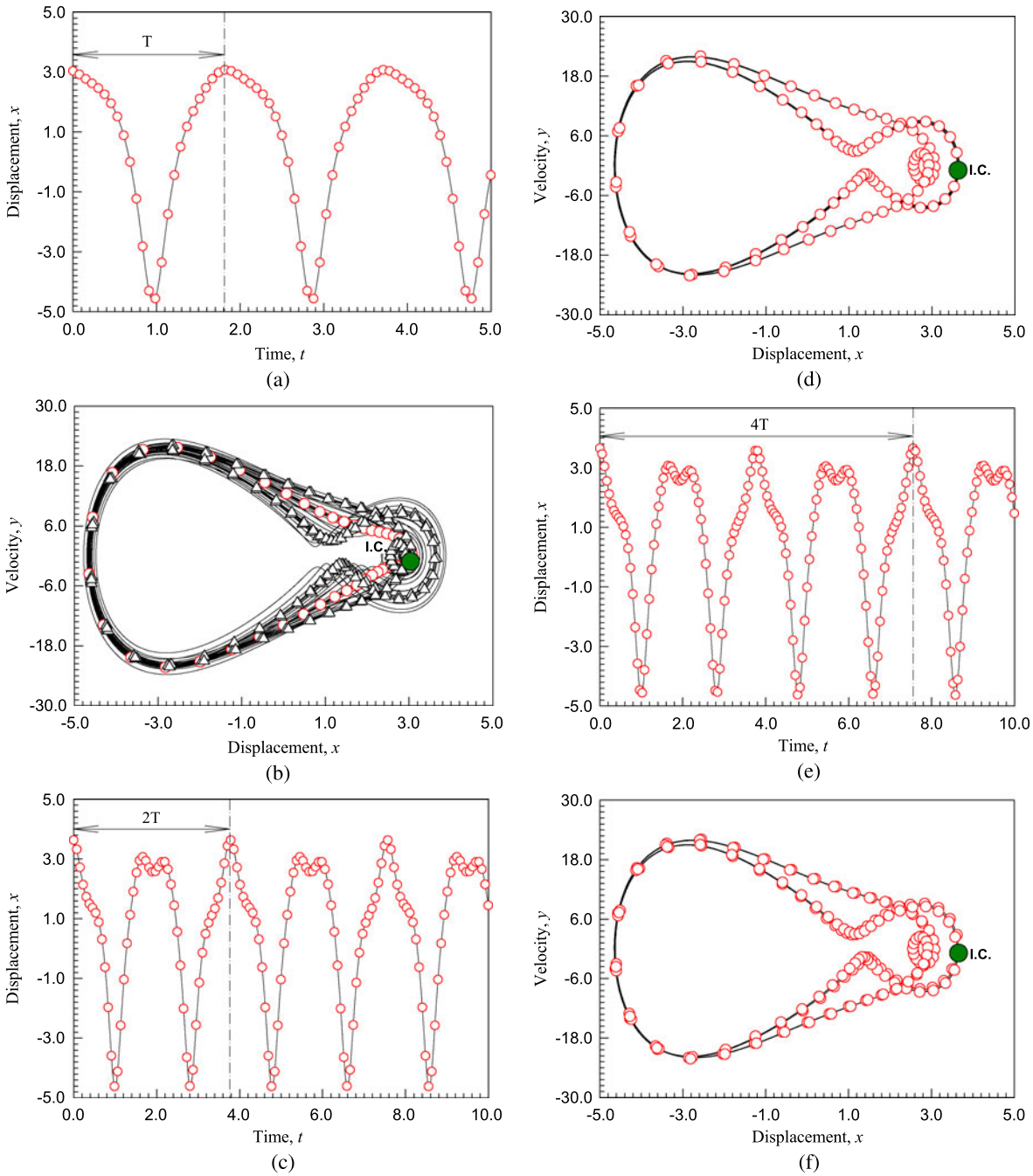

Fig. 9 An unstable, asymmetric period-1 motions (HB10): (**a**) displacement and (**b**) phase plane ($x_0 \approx 3.034700$, $y_0 \approx -1.134240$). An unstable asymmetric period-2 motion (HB20): (**c**) displacement and (**d**) phase plane ($x_0 \approx 3.629530$, $y_0 \approx -0.926901$). A stable period-4 motion (HB40): (**e**) displacement and (**f**) phase plane ($x_0 \approx 3.654920$, $y_0 \approx -0.869122$). ($\Omega = 3.32$, $\delta = 0.2$, $\alpha = 1.0$, $\beta = 4$, $Q_0 = 100.0$)

5 Conclusions

In this paper, the analytical solutions of periodic motions in the periodically forced, hardening Duffing oscillator are obtained. The asymmetric periodic motions for the hardening Duffing oscillators were obtained in order to find chaos in the hardening Duffing oscillator analytically. The bifurcation tree from asymmetric period-1 motions to chaos was presented, and the stable and unstable periodic motions in the hardening Duffing oscillator were presented. The analytical and numerical solutions for stable and unstable periodic motions were illustrated. The results presented in this paper can help one comprehensively understand chaos mechanism in the hardening Duffing oscillator.

References

1. Duffing, G.: Erzwunge Schweingungen bei veranderlicher eigenfrequenz. F. Viewig u. Sohn, Braunschweig (1918)
2. Hayashi, G.: Nonlinear oscillations in Physical Systems. McGraw-Hill Book Company, New York (1964)
3. Nayfeh, A.H.: Perturbation Methods. Wiley, New York (1973)
4. Holmes, P.J., Rand, D.A.: Bifurcations of Duffing equation; An application of catastrophe theory. Q. Appl. Math. **35**, 495–509 (1976)
5. Nayfeh, A.H., Mook, D.T.: Nonlinear Oscillation. Wiley, New York (1979)
6. Holmes, P.J.: A nonlinear oscillator with strange attractor. Philos. Trans. R. Soc. A **292**, 419–448 (1979)
7. Ueda, Y.: Explosion of strange attractors exhibited by the Duffing equations. Ann. N.Y. Acad. Sci. **357**, 422–434 (1980)
8. Coppola, V.T., Rand, R.H.: Averaging using elliptic functions: Approximation of limit cycle. Acta Mech. **81**, 125–142 (1990)
9. Wang, C.S., Kao, Y.H., Huang, J.C., Gou, Y.H.: Potential dependence of the bifurcation structure in generalized Duffing oscillators. Phys. Rev. A **45**, 3471–3485 (1992)
10. Kao, Y.H., Wang, C.S., Yang, T.H.: Influences of harmonic coupling on bifurcations in Duffing oscillator with bounded potential wells. J. Sound Vib. **159**, 13–21 (1992)
11. Janicki, K.L., Szemplinska-Stupnicka, W.: Subharmonic resonances and criteria for escape and chaos in a driven oscillator. J. Sound Vib. **180**, 253–269 (1995)
12. Luo, A.C.J., Han, R.P.S.: A quantitative stability and bifurcation analyses of a generalized Duffing oscillator with strong nonlinearity. J. Franklin Inst. **334B**, 447–459 (1997)
13. Han, R.P.S., Luo, A.C.J.: Comments on "Subharmonic resonances and criteria for escape and chaos in a driven oscillator". J. Sound Vib. **196**(2), 237–242 (1996)
14. Luo, A.C.J., Han, R.P.S.: Analytical predictions of chaos in a nonlinear rod. J. Sound Vib. **227**(2), 523–544 (1999)
15. Peng, Z.K., Lang, Z.Q., Billings, S.A., Tomlinson, G.R.: Comparisons between harmonic balance and nonlinear output frequency response function in nonlinear system analysis. J. Sound Vib. **311**, 56–73 (2008)
16. Luo, A.C.J., Huang, J.Z.: Approximate solutions of periodic motions in nonlinear systems via a generalized harmonic balance. J. Vib. Control **18**, 1661–1674 (2012)
17. Luo, A.C.J., Huang, J.Z.: Analytical dynamics of period-m flows and chaos in nonlinear systems. Int. J. Bifurc. Chaos **22**, 1250093 (29 pages) (2011)
18. Luo, A.C.J.: Continuous Dynamical Systems. HEP-L&H Scientific, Glen Carbon (2012)